

Green Chemistry

Accepted Manuscript



This is an *Accepted Manuscript*, which has been through the Royal Society of Chemistry peer review process and has been accepted for publication.

Accepted Manuscripts are published online shortly after acceptance, before technical editing, formatting and proof reading. Using this free service, authors can make their results available to the community, in citable form, before we publish the edited article. We will replace this *Accepted Manuscript* with the edited and formatted *Advance Article* as soon as it is available.

You can find more information about *Accepted Manuscripts* in the [Information for Authors](#).

Please note that technical editing may introduce minor changes to the text and/or graphics, which may alter content. The journal's standard [Terms & Conditions](#) and the [Ethical guidelines](#) still apply. In no event shall the Royal Society of Chemistry be held responsible for any errors or omissions in this *Accepted Manuscript* or any consequences arising from the use of any information it contains.



www.rsc.org/greenchem

1 like” graphene films are generated *via* simple filtration resulting in films with a conductivity of
2 $2.3 \times 10^4 \text{ S m}^{-1}$, the highest conductivity observed for graphene films assembled *via* vacuum
3 filtration from solution processable graphene sheets to date. After a 2-hour low temperature anneal
4 at 300 °C, the conductivity further increased to $7.4 \times 10^4 \text{ S m}^{-1}$. This eco-friendly and rapid
5 approach for production of highly conductive and “clean” solution-phase graphene sheets would
6 enable a broad spectrum of applications at low cost.

7 **Introduction**

8 Graphene has inspired great enthusiasm for over a decade. Due to its excellent electronic, thermal
9 and mechanical properties along with its exceptionally large surface area and light weight,
10 graphene holds great potential for a wide range of applications.^{1,2} Fundamental studies and high-
11 frequency electronics require pristine graphene.³ “Bulk” applications such as batteries,⁴⁻⁸
12 supercapacitors,⁹ catalysts,^{10, 11} flexible macroelectronics,^{12, 13} and mechanically reinforced
13 conductive coatings,¹⁴⁻¹⁶ require large quantities of high-conductive, solution-processable
14 graphene manufactured at low cost. Mass production of conductive and solution processable
15 graphene sheets, such as reduced graphene oxide (r-GO) and graphene nanoplatelets, has been
16 recently achieved.¹⁷⁻²¹ The majority of r-GO sheets have been fabricated *via* rather complex series
17 of chemical processing steps. First, a lengthy process to oxidize graphite to graphite oxide, which
18 is followed by a thermal exfoliation process accompanied with partial deoxygenation (reduced).
19 The exfoliated and partially reduced graphite is then dispersed into various solvents to obtain
20 solution-processable r-GO.^{22, 23} The other commonly used approach to generate solution-
21 processable r-GO is to first exfoliate and disperse the graphene oxide sheets in solutions and then
22 reduce the GO to a level that restores the conductivity of graphene. The widely used graphite
23 oxidation methods, such as Staudenmaier,²⁴ Hofmann,²⁵ Hummers,²⁶ or Tour’s methods,²⁷ all

1 utilize metal containing oxidants, such as KMnO_4 and/or KClO_3 . Trace residues of these oxidants
2 and metal ions used or generated in these approaches can further participate in undesired reactions
3 and can be detrimental to a wide range of applications.^{14, 28, 29} However, purification of GO remains
4 a challenge, mainly due to its tendency to gel. Even though these metal ions are water soluble, they
5 were trapped due to the gelation tendency of GO, causing the GO product highly flammable.²⁹
6 Therefore, extensive cleaning and purification steps are required making industrial scale
7 production expensive and time-consuming.^{27, 30} Further during thermal exfoliation and
8 deoxygenation of graphite oxide, it was believed that H_2O , CO and CO_2 gases were the only
9 substances released during thermal exfoliation. However, a recent study demonstrated that, a wide
10 variety of complex organic molecules can also be released during processing, including alkanes,
11 substituted polycyclic aromatic hydrocarbons, and heterocyclic molecules. The released molecules
12 pose a potential hazard to our environment if not handled properly. Preventing the formation of
13 these complex wastes is one of the greatest challenge for the graphene industry.³¹ On the other
14 hand, even though environmentally friendly reduction protocols are being developed to reduce
15 dispersed graphene oxide,^{30, 32-35} hydrazine, a hazardous material, is still widely used as the
16 reducing agent. Most importantly, these processes irreparably destroy the ideal honeycomb
17 structure of graphene, leaving only a fraction of the properties of intrinsic graphene to be
18 recovered.³⁶ Finally, except for those which are sulfonyl-functionalized³⁷ or reduced in basic
19 solutions,^{17, 38, 39} highly reduced GO sheets cannot be directly dispersed into water, which is the
20 most useful and sustainable solvent. These sheets have been dispersed either in some organic
21 solvents with high boiling points, such as N-methyl-pyrrolidone (NMP), or in aqueous solutions
22 with the help of surfactants for stabilization.³⁸ Unfortunately, both the organic solvents and the
23 surfactants are difficult to be completely removed from a graphene sheet surface without a high

1 temperature annealing process. Residual solvent and surfactant species inevitably increase contact
2 resistance between individual sheets in graphene films, reducing the overall electrical conductivity
3 of graphene films produced using these chemistries.

4 Several research groups, including our own have reported that defect-free graphene
5 nanoplatelets can be directly produced from graphite particles and dispersed in NMP and other
6 solvents, or aqueous solutions with the help of surfactants for stabilization.^{19, 21, 40, 41} Although the
7 issue of releasing toxic gases was resolved, most of the production requires lengthy sonication and
8 the yield is too low for practical industrial applications. Recently, a more scalable method to
9 produce large-size pristine few-layer graphene was achieved via intercalation of metal containing
10 compounds, followed by an interlayer exfoliation reaction.^{18, 42} These approaches are
11 environmentally friendly and can be used for mass production of large and high quality graphene
12 dispersion in NMP or pyridine, but unfortunately not in aqueous solutions due to the lack of oxygen
13 containing groups on the basal plane of graphene. Therefore the issues associated with high boiling
14 point solvents and trace quantities of metal ions remains.^{29, 43, 44} Oh et al. explored eco-friendly
15 approach to directly produce graphene nanosheets from graphite particles without involving toxic
16 and/or metallic compounds. However, the yield is too low (5%) for practical large scale production.
17 ⁴⁵

18 We recently developed a fast, scalable oxidation approach without involving metallic
19 compounds to directly and controllably produce highly-conductive graphene sheets that can be
20 dispersed in both aqueous and organic solvents without the aid of surfactants.^{46, 47} In that work,
21 KMnO_4 (as is used in Hummers and Tour's methods) was intentionally excluded while nitronium
22 aromatic oxidation combined with microwave heating (fast and local heating) were exploited. The
23 unique process leads to a controllable oxidation of randomly positioned carbon atoms across entire

1 graphene sheets, so that a low density of oxygen containing groups were are shown to be sufficient
2 for exfoliation and dispersion into aqueous solutions. The dispersed graphene sheets, which we
3 refer to as microwave-enabled low oxygen graphene (ME-LOGr), are highly conductive and do
4 not require further reduction. Unfortunately, the use of nitronium ions results in the release of NO₂,
5 a potentially toxic gas.

6 The current work aims to develop a more eco-friendly approach which retains the merits of
7 the nitronium oxidation approach, without releasing toxic gases or generating potentially toxic
8 polycyclic aromatic hydrocarbons. This new approach replaces the mixture of H₂SO₄ and HNO₃
9 and exploits carbon oxidation chemistry by utilizing a piranha solution, a mixture of H₂SO₄ and
10 H₂O₂. Piranha solutions have been widely used in the semiconductor industry and research
11 laboratories to clean silicon, glass, gold, and for oxidative cutting of carbon nanotubes (CNTs).⁴⁸
12 ⁴⁹ The reaction appears to generate only H₂O, O₂, and CO₂, without releasing toxic gases. However,
13 the direct use of piranha solution to oxidize graphite in fabricating large graphene sheets is less
14 efficient than the H₂SO₄/HNO₃ solution. This may be due to the rapid over-oxidation of the surface
15 layers, in part related to the limited ability of the piranha constituents to access the inner graphene
16 layers. This chemistry results in an uncontrolled cutting of graphene sheets at the surface and
17 carbon loss *via* gasification. To solve these problems and to achieve controllable oxidization of
18 each graphene layer, we first prepare a reversible H₂SO₄-graphite intercalation compound (GIC)
19 with the help of (NH₄)₂S₂O₈ *via* a simple room temperature process.⁵⁰ This is followed by a short
20 period of oxygen purging and microwave irradiation in a piranha solution (**Scheme 1**). The synergy
21 of the intercalated oxygen and piranha solution enables controlled oxidation of graphite particles
22 *via* microwave heating and thus leads to rapid (60 seconds) and direct generation of highly
23 conductive low oxygen containing graphene sheets. The intrinsic molecular oxidation mechanism

1 leads to an eco-friendly fabrication of highly conductive graphene sheets without generating toxic
2 byproducts, as demonstrated by GC-MS. To differentiate these films from the ME-LOGr we
3 generated previously by nitronium microwave oxidation, we refer to these graphene sheets as eco-
4 friendly, microwave-enabled low-oxygen graphene (Eco-ME-LOGr). The Eco-ME-LOGr sheets
5 are similar to the ME-LOGr, in that, they can be dispersed in various solvents, including in aqueous
6 solutions, without needing surfactants for stabilization. The sheets are also highly conductive
7 without requiring a post-reduction step. The conductivity of the as-fabricated Eco-ME-LOGr film
8 is $2.3 \times 10^4 \text{ S m}^{-1}$, the highest value reported for graphene films prepared from solution processable
9 graphene sheets *via* a simple vacuum filtration. After 2-hours of low temperature annealing
10 (300°C), the conductivity reaches $7.4 \times 10^4 \text{ S m}^{-1}$. The electrical performance of the Eco-ME-
11 LOGr films significantly outperformed the ME-LOGr films fabricated *via* nitronium microwave
12 oxidation ($6.6 \times 10^3 \text{ S m}^{-1}$ for as-prepared films and $1.9 \times 10^4 \text{ S m}^{-1}$ after 2-hour annealing at
13 300°C).⁴⁶

14 Results and Discussion

15 In a typical experiment, a reversible H_2SO_4 -GIC (instead of H_2SO_4 - HNO_3 GIC) is first
16 formed by exposing graphite particles to a mixture of sulfuric acid and $(\text{NH}_4)_2\text{S}_2\text{O}_8$, following the
17 recipes suggested by Tour's group.⁵⁰ The H_2SO_4 -GIC was purged with O_2 for 5 minutes and then
18 subjected to 60 seconds of microwave irradiation (CEM Discover, 300 watts for smaller scale, and
19 Synthwave from Milestone, 900W for larger scale production, see details in the experimental
20 section and supplementary materials, Figure S1) in a piranha solution. The reaction results in a
21 finely dispersed suspension that is much easier to clean than the paste obtained from Hummer's
22 method.²⁶ The dispersion was cleaned with water *via* vacuum filtration to remove residual H_2SO_4 ,
23 $(\text{NH}_4)_2\text{S}_2\text{O}_8$, and any residual by-products.

1 With the help of bath sonication (30 min), the cleaned filtration cake can be re-dispersed
2 in water to form a colloidal solution without using surfactants or stabilizers. The lateral size and
3 thickness of the dispersed Eco-ME-LOGr sheets were characterized by a scanning transmission
4 electron microscope (STEM), a scanning electron microscope (SEM), and an atomic force
5 microscope (AFM). The thickness of the Eco-ME-LOGr sheets was found to be 0.7-3 nm, between
6 one and a few layers. The sheets have an average lateral size of one to two micrometers with some
7 as large as tens of micrometers across (Figure 1), similar to the ME-LOGr sheets reported earlier.⁴⁶

8 The color of the Eco-ME-LOGr suspension is grayish-black. The UV-Vis-near infrared
9 (NIR) spectrum of the Eco-ME-LOGr solution displayed a plasmon band absorption maximum at
10 a much longer wavelength than GO (268 nm vs. 230 nm) and much stronger absorption in the
11 visible and NIR region (Figure 2A). All of these characteristics are quite different from the typical
12 brown GO solutions (Figure 2A, inset),^{17, 51} yet similar to the previously reported r-GO and ME-
13 LOGr suspensions. These features qualitatively suggest that the as-prepared Eco-ME-LOGr is also
14 similar to the ME-LOGr sheets, containing a large amount of intact graphene domains without
15 requiring a post-reduction procedure.^{17, 19, 52}

16 Raman spectroscopy was utilized to estimate the size of the intact graphene domains. The
17 typical G band, defect D band and 2D band features are shown in the Raman spectrum of the Eco-
18 ME-LOGr film prepared on an anodic filter membrane *via* vacuum filtration (Figure 2B). The
19 intensity ratio of D to G band (I_D/I_G) is 0.75, which is much lower than those of GO and r-GO,^{51,}
20 ⁵³ indicating the high quality of the as-produced graphene sheets by this simple method.
21 Furthermore, the Eco-ME-LOGr sheets also show a strong 2D band, suggesting that these sheets
22 contain little adsorbent-induced surface contamination.^{46, 54}

1 In addition to water, the Eco-ME-LOGr sheets can also be dispersed in polar organic
2 solvents such as NMP (290 mg/L) and N,N-dimethyl formamide (DMF) (200 mg/L), well known
3 solvents to disperse intrinsic graphene sheets and graphene nanoplatelets. Interestingly, even in a
4 nonpolar solvent such as chloroform, in which neither GO, r-GO, nor graphene platelets can be
5 dispersed, the Eco-ME-LOGr can be dispersed with a concentration of 190 mg/L, ten times higher
6 than that of the ME-LOGr sheets (Figure 3 and table S1 in supplementary materials).⁴⁶ It has been
7 reported that the ability of graphene to be dispersed in various solvents is determined primarily by
8 the surface functionalities of the graphene and Hansen parameters of the solvents. Good
9 dispersibility can be reached when all three Hansen solubility parameters (dispersive, polar, and
10 hydrogen-bonding) of a solvent match well with those of the graphene.^{19, 55} The high dispersibility
11 in aqueous and organic (both polar and nonpolar) solvents without requiring surfactants or
12 stabilizers implies that the molecular structure (oxygen containing groups, their relative ratio and
13 distribution on the surface) of the Eco-ME-LOGr sheets is quite different from previously reported
14 GO, r-GO, graphene nanoplatelets.^{56, 57} On the other hand, ME-LOGr disperses well in ethanol
15 and acetone, whereas the Eco-ME-LOGr is barely dispersed, indicating differences on their
16 surface functionalities.⁴⁶

17 The functional groups attached to the Eco-ME-LOGr sheets were studied with X-ray
18 photoelectron spectroscopy (XPS). The C 1s core-level XPS spectrum of Eco-ME-LOGr shows a
19 main peak from oxygen-free carbon and a shoulder resulting from carbon bound to various oxygen
20 species (Figure 4A). The oxygen-free carbon makes up ~76% of the spectrum, similar to that
21 observed for reduced GO sheets^{56, 57} and the ME-LOGr sheets reported previously.⁴⁶ However, the
22 O1s spectrum of Eco-ME-LOGr is different from that of ME-LOGr (Figure 4B and 4C). The O1s
23 spectrum for both the samples were deconvoluted to three or four peaks and their assignment is

1 based on literature values⁵⁸. The peak at 533 eV corresponds to oxygen present either as C-O in
 2 epoxides or anhydrides, or carboxylic groups (due to the very close overlap in binding energies of
 3 these functional groups, it is difficult to distinguish them from each other). The peaks at 532 and
 4 531 eV were assigned to oxygen in hydroxyls and ethers along with carbonyl groups in esters and
 5 anhydrides, and oxygen in carbonyl groups attached to aromatic structures (quinone groups),
 6 respectively. From Table 1, it is apparent that the Eco-ME-LOGr contains more C-O component
 7 in epoxide, anhydrides, and carboxylic groups, whereas, higher percentage of carbonyl groups
 8 exists in the ME-LOGr.

9 **Table 1. Different oxygen containing groups in Eco-ME-LOGr and ME-LOGr**

Functional groups	Binding energy(eV) of O1s	% of each component in Eco-ME-LOGr	% of each component in ME- LOGr
C-O in epoxide, anhydrides and carboxylic acids	533	41	6
C-O in hydroxyls and ethers, C-O with carbonyl groups in esters and anhydrides	532	42	45
C-O in carbonyl groups attached to aromatic structures (quinones)	531	18	43
Water	536	0	5

10

11 The conductivity of the Eco-ME-LOGr sheets was also studied. It has been reported that the
 12 conductivity of graphene films formed from graphene dispersions exhibit percolation behavior.⁵⁹
 13 The percolation threshold and the conductivity after percolation of graphene films are determined
 14 by the conductivity of the individual graphene sheets (itself a function of extent of

1 functionalization as well as their structure) and by their electrical connectivity (number of contacts
2 and the contact resistance between individual sheets in the films). Films of different thicknesses
3 from the Eco-ME-LOGr aqueous suspension were prepared by vacuum filtration, a common
4 technique to make relatively uniform films from solution phase graphene sheets.^{57, 60} Under a
5 filtration-induced directional flow, graphene films are formed by stacking and interlocking of
6 individual sheets.⁵⁷ After drying in vacuum at room temperature, the average thickness of each
7 film was estimated from the areal density of the films measured with Rutherford Backscattering
8 Spectroscopy (RBS, see details in supplementary materials).⁴⁶ The sheet resistance of the films
9 was measured with a four-probe approach. As shown in Figure 5, the sheet resistance of the Eco-
10 ME-LOGr film decreases with increasing film thickness. The electronic percolation of the Eco-
11 ME-LOGr films was obtained at a thickness of ~88 nm, which has a sheet resistance of 0.5
12 k Ω /square, corresponding to a DC conductivity of 2.3×10^4 S/m. This conductivity is significantly
13 higher than all of the chemically reduced GO films reported (see Table 2). It should be noted that
14 the r-GO films listed here were obtained from stable r-GO aqueous suspensions without surfactants,
15 so that their low conductivities are not due to surfactant or solvent effects.^{17, 38, 39} The high quality
16 of the Eco-ME-LOGr (the existence of larger intact graphene domains and fewer defects indicated
17 by the low I_D/I_G ratio and strong 2D band in its Raman spectrum) likely contributes to the observed
18 high conductivity. This conductivity is also significantly higher than the graphene sheets directly
19 exfoliated in NMP and other organic solvents, as well as in aqueous solutions in the presence of
20 surfactants/stabilizers, even though they were known to have lower defect densities.^{19, 41} The clean
21 surface of Eco-ME-LOGr conveys better electronic communication between individual sheets
22 when they were assembled into a film. Overall, the combination of the high conductivity of

1 individual sheets and low inter-sheet contact resistance leads to the high conductivity of the Eco-
 2 ME-LOGr films.

3

4

5 **Table 2. Electrical conductivity of graphene films prepared via vacuum filtration of different**
 6 **solution phase graphene sheets.**

Fabrication techniques	Conductivity(S/m)
Eco-ME-LOGr	22,600
ME-LOGr ⁴²	6600
Reduced graphene oxide via hydrazine at basic conditions ^{17,55}	7200
Reduced graphene oxide via hydrazine in the presence of Pyrene derivatives ⁶¹	200
Flash reduced GO ⁶³	1000
Reduced K-modified reduced GO ³⁶	690
Sulfonyl modified Reduced Graphene oxide in aqueous ³⁴	17
Electrochemical reduction of graphene oxide ⁶²	3500
Reduced GO in variety of organic solvent mixures ³⁵	1700
Solvothermal reduction of graphene oxide in NMP ¹⁴	374
Graphene nanoplatelets in NMP ¹⁹	5
Graphene nanoplatelets dispersed in aqueous solution via sonication with pyrene derivatives ³⁷	1900-2150
Graphene nanoplatelets dispersed in aqueous solution via sonication with sodium dodecyl benzene sulfate ³⁸	35

7

1 Thermal annealing has been used to enhance the conductivity of graphene films by
2 evaporating residual solvent/surfactant molecules, and/or thermal deoxygenation of the oxygen
3 containing groups. Upon annealing the Eco-ME-LOGr film at 300°C in Ar for 2 hours, the
4 conductivity further increased to $7.44 \times 10^4 \text{ S m}^{-1}$, which is significantly higher than similar r-GO
5 films (Table 3). Although GO films can be directly converted to conductive films via thermal
6 annealing, the electrical conductivity of thermally treated GO films was found to be much lower
7 than annealed r-GO films.⁶⁰ Recently, the evolution of carbon bonds in GO films upon thermal
8 annealing has been carefully studied by molecular dynamic simulations and *in situ* spectroscopic
9 techniques (XPS and infrared spectroscopy) as a function of the initial oxygen density in GO films
10 and annealing temperatures.^{56, 61} It was revealed that significant atomic rearrangement took place
11 and the GO sheets were substantially disordered after thermal annealing, with the highest initial
12 oxygen content resulting in the most severe distortion. In contrast, thermal annealing improved the
13 ordering of the graphene sheets due to the initial low oxygen concentration of the chemically
14 reduced GO films. It also gave rise to additional deoxygenation of the sheets. The improved
15 ordering and additional deoxygenation in the chemically reduced GO films have been ascribed to
16 the observed higher conductivity than the directly annealed GO films.^{38, 60} It is noteworthy that the
17 conductivity of the annealed Eco-ME-LOGr film at 300°C is six times higher than the r-GO films
18 annealed at 220°C and two times higher than the r-GO annealed at 500 °C.⁶⁰ This result strongly
19 demonstrates that even though the oxygen content is similar to that in r-GO, the high quality (less
20 defective structure) of Eco-ME-LOGr makes it much easier to recover the pristine electronic
21 properties of graphene.

22 It should also be noted that the conductivity of the Eco-ME-LOGr films outperformed our
23 ME-LOGr films as indicated by: a thinner percolation threshold (88 nm vs. 200 nm), lower sheet

1 resistance at percolation threshold (0.5 vs. 0.76 k Ω /square), which corresponds to the much higher
 2 DC conductivity (2.26×10^4 S/m vs. 6.6×10^3 S/m) for as-prepared films. After 2-hour annealing
 3 at 300 $^\circ$ C, the conductivity of the Eco-ME-LOGr films and the ME-LOGr films increased to $7.44 \times$
 4 10^4 S/m vs. 1.92×10^4 S/m, respectively.⁴⁶

6 **Table 3. Electrical conductivity of graphene films after low temperature thermal annealing.**

Graphene dispersion technique	Annealing temperature	Conductivity(S/m)
Eco-ME-LOGr	300 $^\circ$ C for 2hrs with Ar	74,400
ME-LOGr ⁴²	300 $^\circ$ C for 2hrs with Ar	19,200
Reduced graphene oxide via hydrazine at basic conditions ^{17,55}	220 $^\circ$ C for 2hrs with Ar	11,800
	500 $^\circ$ C for 2hrs with Ar	35,100
Reduced GO in variety of organic solvent mixures ³⁵	150 $^\circ$ C for 12hrs	16,000
Solvothermal reduction of graphene oxide in NMP ¹⁴	250 $^\circ$ C for 2hrs	1380
Graphene nanoplatelets in NMP ¹⁹	300 $^\circ$ C for 2hrs with Ar	5000
	250 $^\circ$ C for 2hrs with Ar/H ₂	6500

8
 9
 10 We emphasize not only on the significantly high conductivity of the Eco-ME-LOGr films,
 11 but also that the chemistry to fabricate these high quality graphene sheets is eco-friendly without
 12 generating toxic gases and byproducts. First, we found that the gas released during the reaction
 13 was colorless, which was expected as no nitronium ions are involved in the piranha/O₂ oxidation
 14 approach. Surprisingly, the filtrate was also colorless, which is significantly different from the
 15 yellow/brown filtrates obtained from nitronium oxidation (Figure 6B, inset). Gas chromatography-

1 mass spectroscopy (GC-MS) was used to carefully study the composition of the released gas phase
2 and the byproducts in the filtrates collected during cleaning of the microwave oxidized products.
3 The gas phase collected during the microwave oxidation was directly injected to GC-MS. The
4 results show that the majority of the components were O₂ and a small amount of CO₂; no toxic
5 SO₂ and CO were detected. Note that the 28m/z peak is assigned to N₂, not to CO as the GC-MS
6 does not exhibit a strong carbon peak at 12m/z which is characteristic for a CO spectrum (Figure
7 6A).

8 To study the components in the filtrate (collected during cleaning of the microwaved product),
9 it was first mixed with a low boiling point polar organic solvent, such as tetrahydrofuran (THF)
10 before injection. For comparison, the filtrate from nitronium oxidation and a blank solution
11 (obtained by microwave irradiation of the same amount of (NH₄)₂S₂O₈ and piranha solution but
12 without graphite particles) were also studied. In Figure 6B, the chromatogram of the filtrate from
13 nitronium oxidation shows several peaks at retention times of 1.5 min, 4.17min, 7.49min and 11.78
14 min. The mass spectra (MS) for each of the peaks were collected and are shown in Supplementary
15 Materials (Figure S8). The molecular structures associated with the peaks were identified based
16 on the score (max score is 1.00) of the MS compared to spectra in the mass bank database. The
17 peak at 1.5 min is mainly from THF and the peak at 4.17 min is most likely from flavanol
18 derivatives, while the peaks at 7.49 min and 11.78 min were due to relatively high molecular
19 weight compounds like cyanine or 1,1'-dianthrimide. Detailed molecular structures and their
20 scores are given in supplementary materials (Table S3). In marked contrast, the GC of the filtrate
21 of the piranha oxidation approach is similar to that of the blank solution. Only one peak from the
22 solvent (THF) itself was observed, demonstrating that, this new piranha/O₂ oxidation approach is

1 indeed eco-friendly without releasing any detectable toxic gases and generating any potentially
2 toxic aromatic byproducts.

3 In general, an efficient approach to controllably fabricate graphene sheets from graphite
4 requires the following conditions: (1) enabling the oxidant molecules to access internal surfaces
5 of graphite particles (Due to the strong interaction and close distance between the sheets, only the
6 edges of graphite particles and the exposed graphene surface are readily accessible to oxidants; the
7 rest of the graphene is simply physically blocked from interacting with the oxidant molecules);⁶²
8 (2) ensuring that the reactions proceed in a manner such that oxygen containing groups (or other
9 solubilizing groups) can be evenly (or at least randomly) placed across the graphene to have
10 strong interactions with solvent molecules for dispersion; and (3) generating oxygenated groups
11 in a controlled manner such that the process does not cut the graphene sheets into small pieces. In
12 addition, the oxidation of each layer of graphene includes several steps: Firstly, oxidation is
13 initiated to create oxygen containing groups, such as -OH and/or epoxy groups, on the basal plane
14 and edges of graphene sheets. Further oxidation includes two simultaneous and competing
15 processes: (i) continuing initiation of oxidation in the intrinsic graphene domains resulting in
16 generation of more -OH and/or epoxy groups; and/or (ii) further oxidation of the already oxidized
17 carbon atoms, ultimately leading to gasification of the carbon atoms (mostly CO or CO₂) and
18 generation of small carbon residual species (which are separated during filtration), resulting in
19 vacancies and holes throughout the graphene basal planes. This process is referred to as defect
20 consumption or etching.^{48, 63} Consumption of the defects and generation of vacancies and holes in
21 graphene sheets lead to rapid cutting of the CNTs into short pipes and cutting graphene sheets to
22 small pieces.^{48, 49} The relative reaction rates of these processes determine the overall speed of the
23 graphene fabrication and also the lateral sizes and oxidation level of the fabricated graphene sheets.

1 The molecular mechanism leading to all those different results compared to the nitronium
2 oxidation approach needs further studies. We hypothesize that, the difference arises due to their
3 different intercalation capabilities, initial oxidation mechanisms and the following oxidization
4 pathways. The mechanism for nitronium oxidation approach is discussed in detail in our previous
5 reports.⁴⁶ There is no detailed study of the piranha oxidation mechanism even though it has been
6 used to oxidize and cut carbon nanotubes (CNTs).^{49, 64 65} It has been proposed that the most likely
7 route by which piranha oxidation occurs is *via* the generation of atomic oxygen, which directly
8 attacks a carbon in a graphene sheet to form a carbonyl group.⁶⁶ With the formation of carbonyl
9 groups, the bonds of neighboring carbon atoms get disrupted. With further oxidation, the generated
10 carbonyl group can be converted into CO₂, and simultaneously a new carbonyl group is created on
11 a neighboring carbon atom. Compared to oxidation by nitronium ions, oxidation by piranha
12 solution only generates water, CO₂ and O₂ as byproducts. If H₂SO₄/H₂O₂ can be used to oxidize
13 graphite and fabricate graphene sheets, the issue of toxic by-products will be solved.

14 However, our results demonstrated that direct replacement of HNO₃/H₂SO₄ with piranha
15 solution to efficiently fabricate conductive graphene in aqueous solution was not successful. The
16 concentration of the dispersed graphene nanosheets is low (0.1 mg/ml). A majority of the graphite
17 particles are precipitated out. This suggests that only small amounts of graphene sheets, which are
18 located on the surface of the graphite particles were oxidized. This result indicates that the atomic
19 oxygen from piranha solution is different from nitronium ions and has limited capability to reach
20 and oxidize the internal sites of the graphite particles. Furthermore, most of the dispersed sheets
21 are smaller than 200 nm, suggesting the oxidized sheets were quickly cut to small pieces (Figure
22 1D). It was reported that at room temperature H₂SO₄/H₂O₂ is not able to initiate oxidation of the
23 graphene sidewall of carbon nanotubes, while it has much faster speed to etch away the defects

1 thus, cutting the tubes into small pipes compared to nitronium ions.^{48,49} Even though the capability
2 of H₂SO₄/H₂O₂ to initiate oxidation is increased with the microwave heating (high reaction
3 temperature is achieved), it is very possible that the etching speed increased more dramatically.
4 As a result, the oxidized graphene sheets were quickly cut to small pieces.

5 To let the oxygen radicals access the inner parts of graphite particles, we thought to take
6 advantage of the enlarged distance between graphene sheets in a graphite intercalation compound
7 (GIC). It was reported that exposing graphite powders to a mixture of (NH₄)₂S₂O₈ and H₂SO₄ at
8 room-temperature leads to formation of a reversible sulfuric acid-based GIC.⁵⁰ During GIC
9 formation, positive charges were generated in the graphene sheets, which were balanced with
10 intercalated HSO₄⁻ ions. Both HSO₄⁻ ions and H₂SO₄ molecules were intercalated in the interlayer
11 galleries of the GIC. However, the efficiency of oxidation improved marginally, indicated by
12 slightly increased graphene concentration (0.17 mg/ml), while the size of the sheets still remained
13 very small (< 200 nm) (Supplementary Materials, Figure S2 A). It was reported that the H₂SO₄-
14 GIC formed from (NH₄)₂S₂O₈ is reversible since there were no C-O bonds formed. With water
15 washing, the intercalated HSO₄⁻ and H₂SO₄ could be quickly de-intercalated.⁵⁰ Since the H₂O₂
16 solution contains 70% of water (by wt), possibly large amount of HSO₄²⁻ and H₂SO₄ were already
17 de-intercalated before the O· radicals reach the inner graphitic particles.

18 To keep the enlarged distance in the GIC for O· radicals internalization, we purged O₂ to the
19 freshly prepared GIC before exposing them into the piranha solution. We hypothesize the distance
20 between graphene sheets in the GIC is large enough for O₂ intercalation. Further, due to the high
21 electronegativity of O₂, a strong attractive interaction between O₂ and the positive charges on the
22 graphene sheets should exist, which would further facilitate O₂ intercalation and prevent its de-
23 intercalation when the GIC is exposed to an aqueous environment. To study if purging O₂ would

1 help to stabilize the GIC against de-intercalation, we compared the weight of the GICs with and
2 without O₂ purging after water cleaning. The weight of the GIC with O₂ purging remained larger
3 extents compared to the one without experiencing O₂ purging supporting our assumption
4 (Supplementary Materials, Table S2). Therefore, it is very likely that the larger distances between
5 graphene sheets in the GIC are largely remained compared to those without O₂ purging.
6 Accordingly, oxidation of both internal and external graphene sheets in a graphitic particle is
7 expected upon addition of piranha solution and followed by microwave irradiation.

8 Furthermore, it was reported that, trace amounts of C-O bonds were detected after keeping
9 the reversible GIC in its parent (NH₄)₂S₂O₈-H₂SO₄ solution at ambient conditions for seven days.⁵⁰
10 Molecular level understanding of the chemical reaction of reversible GIC with oxygen in highly
11 acidic solution has not been extensively studied. We propose that the O₂ in air may intercalate and
12 absorb around the positive charges, which can promote an electron/oxygen transfer reaction
13 between the absorbed molecular oxygen and the positively charged graphene, leading to gradual
14 generation of few epoxy groups, a scenario similar to the nitronium ion intercalated GIC.⁴⁶
15 Considering higher concentration of O₂ may be intercalated into the galleries of GIC along with
16 the rapidly increased temperature *via* microwave heating, multiple oxygen containing groups can
17 be efficiently generated not only along the edges, but also across the basal plane of graphene sheets
18 *via* oxygen transfer reactions.^{67, 68} The synergy of intercalated oxygen and piranha may lead to
19 increased speed in generating oxygen-containing groups relatively to the cutting speed. Therefore,
20 a higher yield of graphene production and less carbon loss were expected. Indeed, not only the
21 concentration of graphene sheets is increased, but also the lateral sizes of the graphene sheet was
22 also increased dramatically (Figure 1).

1 A control experiment was performed by directly microwave heating the O₂ purged GIC
2 without adding piranha solution. The results demonstrated that relatively larger graphene sheets
3 were obtained compared to those obtained *via* piranha oxidation of GIC without O₂ purging.
4 However, the obtained graphene sheets are much thicker while having smoother edges compared
5 to the ones obtained in the presence of piranha solution (Supplementary materials, Figure S3). It
6 should also be mentioned that, purging O₂ directly to a mixture of H₂SO₄/graphite particles did not
7 produce large graphene sheets, presumably, due to the small distance between graphene sheets in
8 graphite particles for O₂ intercalation. Furthermore, since there are no positive charges on graphene
9 sheets in pristine graphite particles, there is no driving force for O₂ to internalize without forming
10 a GIC in the first place. On the other hand, however, purging O₂ for longer times with piranha
11 solution and/or increasing the microwave irradiation time caused a significant decrease in the
12 lateral sizes of the graphene sheets, or even more carbon loss, possibly due to over-oxidation
13 induced cutting and etching (supplementary materials, Figure S4-5).⁴⁸ In addition, the size and
14 yield of the graphene sheets also depend on the ratio of H₂O₂/H₂SO₄ and the microwave power.
15 Increasing the ratio of H₂O₂/H₂SO₄ and decreasing the microwave power results in deficient
16 oxidation and most of the graphite particles precipitate out (supplementary materials, Figure S6-
17 7).

18 Finally, due to the different molecular oxidation mechanisms and their different kinetics in
19 the initiation and the following oxidation pathways, we found the role of microwave heating in
20 these two approaches also varied. In nitronium oxidation approach, microwave heating enables
21 direct production of highly conductive graphene sheets without the requirement of post reduction
22 process, while traditional heating results in nonconductive graphene oxide nanosheets. On the
23 contrary, both traditional heating and microwave heating lead to highly conductive graphene sheets

1 via the piranha/O₂ oxidation chemistry. The graphene sheets produced via microwave heating are
2 much larger (several μm) than the ones from traditional heating (< 200 nm) (supplementary
3 materials (Figure S2 D)).

4 **Conclusion**

5 In summary, by formation of reversible GIC, the distance between graphene sheets is increased
6 simultaneously with the generation of positive charges on the graphene sheets, which provides
7 enough space and imparts a strong attractive driving force for O₂ intercalation. The interaction
8 between the positive charges and O₂ also helps in stabilizing the intercalated O₂ and HSO₄⁻ ions
9 against de-intercalation upon introduction of the piranha solution. The existence of the intercalated
10 O₂ not only maintains the distance for piranha to access and oxidize the inner parts of graphite
11 particles, but also acts as a mild oxidant to generate more oxygen containing groups on the
12 graphene sheets which facilitates graphene sheet dispersion into aqueous solutions. The synergy
13 of the piranha generated oxygen radicals, the intercalated O₂ and microwave heating enables rapid
14 (60 seconds), direct and controllable fabrication of highly conductive graphene sheets of different
15 lateral sizes without requiring post reduction procedure. The intrinsic oxidation mechanism of this
16 new approach ensures that toxic by-products such as aromatic molecules or gas are not generated. .
17 Finally, the unique microwave heating not only enhances the fabrication process but also facilitates
18 larger graphene sheets production compared to those utilizing traditional heating. Collectively, this
19 approach has the following advantages for mass production of high quality graphene dispersions:
20 (1) eco-friendly, no toxic agents are involved (2) Rapid and low energy consuming fabrication
21 process (3) direct production of graphene sheets of different lateral sizes without the requirement
22 for a post-reduction process. The as fabricated graphene sheets have a lower level of oxygen-
23 containing groups, which ensures substantial reservation of the outstanding electrical and optical

1 properties without the need for a high temperature annealing process;⁵⁶ (4) high-concentration
2 dispersions both in aqueous and organic solvents (without requiring polymeric or surfactant
3 stabilizers) allows a “clean” graphene surface to be obtained; (5) reduced waste from purification
4 steps; (6) since only $(\text{NH}_4)_2\text{S}_2\text{O}_8$, O_2 , H_2SO_4 and H_2O_2 are used for the production, the byproducts
5 are essentially $(\text{NH}_4)_2\text{SO}_4$, and diluted H_2SO_4 , which can be reused to produce more $(\text{NH}_4)_2\text{SO}_4$ as
6 soil fertilizers. All these advantages ensure mass production of high quality graphene dispersions
7 with low environmental footprints and at a much lower-cost (The waste generated and energy
8 consumed in the current process were roughly estimated and compared with other routine r-GO
9 fabrication, clearly illustrating the green process reported in this work, see more detail in the
10 supporting information).

11 **Experimental Method:**

12 **Materials.**

13 The Synthetic Graphite powder (size $\leq 20\mu\text{m}$) and ammonium persulfate (reagent grade
14 98%) were obtained from Sigma Aldrich. The concentration of sulfuric acid used is 98% and is
15 obtained from Pharmaco Aaper. The H_2O_2 is a laboratory grade solution with a concentration of
16 wt 35% obtained from BDH. All the chemicals were used as received. The extra dry grade O_2 is
17 used for O_2 purging. The small-scale graphene synthesis was conducted *via* CEM discover
18 microwave vessel whereas the large scale synthesis was conducted *via* Synthwave from Milestone.
19 Dispersion of the microwaved graphite powers to graphene sheets into various solvents was
20 performed *via* 5210 bath sonicator.

21 **Eco-friendly approach for fabrication of graphene sheets**

1 Graphite intercalation compound with SO_4^{2-} is achieved by following the method as
2 described by Tour et al.⁵⁰ In brief, 1000mg of ammonium persulfate $[(\text{NH}_4)_2\text{S}_2\text{O}_8]$ was dissolved
3 in 10ml H_2SO_4 . The obtained mixture solution was stirred for 5-10 mins and then 200mg of
4 Graphite powder was added. The obtained mixture was stirred for 24hrs, which led to the formation
5 of Graphite intercalation Compound (reversible SO_4^{2-} -GIC). To the GIC- SO_4 solution, oxygen is
6 purged for 5mins at a rate of 79-84 ml/min. 1ml of the O_2 purged GIC- SO_4 solution is taken and
7 mixed with 9ml of Piranha solution (H_2SO_4 : H_2O_2 = 3:1), which is microwaved at 300W for 60sec.
8 The reaction is initially quenched with 200ml deionized water. The obtained slurry was washed
9 *via* vacuum filtration through a polycarbonate membrane with a pore size of $0.8\mu\text{m}$ with 200ml
10 water each for four times. The final product is dispersed in 40ml deionized water by sonication in
11 a bath sonicator for 30mins. The solution is allowed to settle for 3-5days and the supernatant
12 solution obtained contains large graphene sheets. The filtrate is collected and then extracted with
13 THF to study the byproducts *via* gas chromatography-mass spectrometry (GC-MS)

14 To demonstrate that this approach can be scaled up for mass production, 10ml of graphite
15 intercalated solution, which is purged with O_2 for 5mins, is taken and to it add 90ml of Piranha
16 solution (H_2SO_4 : H_2O_2 - 3:1) and microwave at 900W for 60sec with Synthwave from Milestone.
17 The quenching and cleaning of the product is similar to the small scale fabrication. The microwave
18 enabled nitronium oxidation approach of graphene synthesis is conducted according to the
19 procedure described in our previous work.⁴⁶ However the starting material is the graphite
20 intercalated compound. The traditional heating of the piranha trial is conducted by heating 1ml of
21 O_2 purged GIC with 9ml of Piranha solution at 100°C for 7hrs and then quenching the reaction
22 mixture with 200ml deionized water and washing it with 200ml water each for four times.

23 **Characterization techniques:**

1 **Surface Morphology:** The surface morphology of our as fabricated product is characterized by
2 an Atomic force Microscopy using a Nanoscope IIIa multimode SPM (Digital instruments)
3 operated in “Tapping mode” and Scanning Electron Microscopy (SEM) and scanning
4 Transmission Electron Microscopy (STEM) using a Hitachi S-4800 Field Emission Scanning
5 Electron Microscope (FE-SEM, Hitachi Co.Ltd.). The functional groups information was acquired
6 using a thermo scientific K α system with a monochromated Al K α X-ray source ($h\nu=1486.7\text{ev}$)
7 in XPS. The quality of the graphene sheets were analyzed using a Raman spectra with a Kaiser
8 Optical Systems Raman Microprobe.

9 **Optical and Electronic properties:** The optical properties of the graphene dispersions were
10 measured by the UV-VIS NIR spectroscopy from Cary-5000 Ultra violet-Visible-Near Infrared
11 Spectroscopy operated in double beam with 200-1000nm wavelength range. As for the electronic
12 properties assessment, the sheet resistance is measured by a manual four point resistivity probe
13 from Lucas Laboratories, model 302. The conductivity of the films is calculated from the sheet
14 resistance and thickness by the formula:

$$15 \quad \text{Conductivity} = \frac{1}{\text{Sheet resistance} \times \text{thickness}}$$

16 Rutherford back scattering (RBS) was performed to calculate the thickness of the film to obtain
17 the conductivity of the as prepared graphene film, using a 2 MeV He²⁺ ion beam produced in a
18 tandem accelerator with an ion current of 2–3 nA. Spectra were collected in the back scattering
19 geometry and simulations were performed using the SIMNRA program (see detail in
20 supplementary materials).

21 **Gas Chromatography-Mass Spectrometry (GC-MS).** The gas evolved during and the reaction
22 process and the filtrate during cleaning procedure are carefully collected and analyzed using an

1 Agilent HP6890 system, which was equipped with a HP-5-MS capillary column. The sample
2 preparation procedure for the characterization techniques is discussed in detail in the
3 supplementary information.

4 *Conflict of Interest:* The authors declare no competing financial interest.

5 **Acknowledgment:** This material is based upon work supported by the National Science
6 Foundation under Grant STTR-1346496 (KS, AW and HH).

7 **Notes and References**

8 ¹Chemistry Department, Rutgers University, Newark, NJ 07102

9 ²Department of Chemistry and Chemical Biology, Rutgers University, 610 Taylor Rd, Piscataway,
10 NJ 0885

11 ³Ocean Nanotech LLC, 7964 Arjons Drive, Suite G, San Diego, CA 92126.

12 **Electronic supplementary Information Available:** Data for larger scale production of Eco-ME-
13 LOGr; concentration and production yield of the Eco-ME-LOGr in different solvents; lateral sizes
14 and yields depending on microwave power; microwave irradiation time; O₂ purging time; and
15 H₂SO₄/H₂O₂ ratio; detailed mass spectra and possible assignment of the peaks showing on the GC
16 spectrum of the filtrates at different retention time; principle and data treatment of thickness
17 measurement *via* Rutherford Back Scattering (RBS).

18 **References**

- 19 1. K. S. Novoselov, V. I. Fal'ko, L. Colombo, P. R. Gellert, M. G. Schwab and K. Kim, *Nature*, 2012, **490**,
20 192-200.
- 21 2. F. Bonaccorso, A. Lombardo, T. Hasan, Z. Sun, L. Colombo and A. Ferrari, *Materials Today*, 2013,
22 **15**, 564-589.
- 23 3. Y. Q. Wu, Y. M. Lin, A. A. Bol, K. A. Jenkins, F. N. Xia, D. B. Farmer, Y. Zhu and P. Avouris, *Nature*,
24 2011, **472**, 74-78.

- 1 4. K. Han, J. M. Shen, C. M. Hayner, H. Q. Ye, M. C. Kung and H. H. Kung, *Journal of Power Sources*,
2 2014, **251**, 331-337.
- 3 5. L. L. Jiang and Z. J. Fan, *Nanoscale*, 2014, **6**, 1922-1945.
- 4 6. H. Kim, H. D. Lim, J. Kim and K. Kang, *Journal of Materials Chemistry A*, 2014, **2**, 33-47.
- 5 7. A. H. Li, J. Q. Liu and S. Y. Feng, *Science of Advanced Materials*, 2014, **6**, 209-234.
- 6 8. N. Mahmood, C. Z. Zhang, H. Yin and Y. L. Hou, *Journal of Materials Chemistry A*, 2014, **2**, 15-32.
- 7 9. Z. J. Jiang, Z. Q. Jiang and W. H. Chen, *Journal of Power Sources*, 2014, **251**, 55-65.
- 8 10. Y. Zhu, S. Murali, M. D. Stoller, K. J. Ganesh, W. Cai, P. J. Ferreira, A. Pirkle, R. M. Wallace, K. A.
9 Cychosz, M. Thommes, D. Su, E. A. Stach and R. S. Ruoff, *Science*, 2011, **332**, 1537-1541.
- 10 11. Z. Jin, W. Lu, K. J. O'Neill, P. A. Parilla, L. J. Simpson, C. Kittrell and J. M. Tour, *Chemistry of Materials*,
11 2011, **23**, 923-925.
- 12 12. G. Eda and M. Chhowalla, *Advanced Materials*, 2010, **22**, 2392-2415.
- 13 13. P. H. Wobkenberg, G. Eda, D. S. Leem, J. C. de Mello, D. D. C. Bradley, M. Chhowalla and T. D.
14 Anthopoulos, *Advanced Materials*, 2011, **23**, 1558-1562.
- 15 14. S. Dubin, S. Gilje, K. Wang, V. C. Tung, K. Cha, A. S. Hall, J. Farrar, R. Varshneya, Y. Yang and R. B.
16 Kaner, *ACS Nano*, 2010, **4**, 3845-3852.
- 17 15. S. Stankovich, D. A. Dikin, G. H. B. Dommett, K. M. Kohlhaas, E. J. Zimney, E. A. Stach, R. D. Piner,
18 S. T. Nguyen and R. S. Ruoff, *Nature*, 2006, **442**, 282-286.
- 19 16. T. Ramanathan, A. A. Abdala, S. Stankovich, D. A. Dikin, M. Herrera-Alonso, R. D. Piner, D. H.
20 Adamson, H. C. Schniepp, X. Chen, R. S. Ruoff, S. T. Nguyen, I. A. Aksay, R. K. Prud'homme and L.
21 C. Brinson, *Nature Nanotechnology*, 2008, **3**, 327-331.
- 22 17. D. Li, M. B. Muller, S. Gilje, R. B. Kaner and G. G. Wallace, *Nature Nanotechnology*, 2008, **3**, 101-
23 105.
- 24 18. X. Geng, Y. G. Guo, D. Li, C. Zhu, X. Wei, M. N. Chen, S. Gao, S. Qiu, Y. Gong, L. Wu, M. Long, M.
25 Sun, G. Pan and L. Liu, *Science Reports*, 2013, **3**, 1134.
- 26 19. Y. Hernandez, V. Nicolosi, M. Lotya, F. M. Blighe, Z. Y. Sun, S. De, I. T. McGovern, B. Holland, M.
27 Byrne, Y. K. Gun'Ko, J. J. Boland, P. Niraj, G. Duesberg, S. Krishnamurthy, S. Goodhue, J. Hutchison,
28 V. Scardaci, A. C. Ferrari and J. N. Coleman, *Nature Nanotech.*, 2008, **3**, 563 - 568.
- 29 20. S. Park and R. S. Ruoff, *Nature Nanotech.*, 2009, **4**, 217-224.
- 30 21. K. R. Paton, E. Varrla, C. Backes, R. J. Smith, U. Khan, A. O'Neill, C. Boland, M. Lotya, O. M. Istrate,
31 P. King, T. Higgins, S. Barwich, P. May, P. Puczkarski, I. Ahmed, M. Moebius, H. Pettersson, E. Long,
32 J. Coelho, S. E. O'Brien, E. K. McGuire, B. M. Sanchez, G. S. Duesberg, N. McEvoy, T. J. Pennycook,
33 C. Downing, A. Crossley, V. Nicolosi and J. N. Coleman, *Nat Mater*, 2014, **13**, 624-630.
- 34 22. H. C. Schniepp, J. L. Li, M. J. McAllister, H. Sai, M. Herrera-Alonso, D. H. Adamson, R. K.
35 Prud'homme, R. Car, D. A. Saville and I. A. Aksay, *Journal of Physical Chemistry B*, 2006, **110**, 8535-
36 8539.
- 37 23. M. J. McAllister, J. L. Li, D. H. Adamson, H. C. Schniepp, A. A. Abdala, J. Liu, M. Herrera-Alonso, D.
38 L. Milius, R. Car, R. K. Prud'homme and I. A. Aksay, *Chemistry of Materials*, 2007, **19**, 4396-4404.
- 39 24. L. Staudenmaier, *Berichte Der Deutschen Chemischen Gesellschaft*, 1898, **31**, 1481-1487.
- 40 25. U. Hofmann and E. Konig, *Z. Anorg. Allg. Chem.*, 1937, **234**, 311.
- 41 26. W. S. Hummers and R. E. Offeman, *J. Am. Chem. Soc.*, 1958, **80**, 1339-1339
- 42 27. D. C. Marcano, D. V. Kosynkin, J. M. Berlin, A. Sinitskii, Z. Z. Sun, A. Slesarev, L. B. Alemany, W. Lu
43 and J. M. Tour, *ACS Nano*, 2010, **4**, 4806-4814.
- 44 28. S. J. You, S. M. Luzan, T. Szabo and A. V. Talyzin, *Carbon*, 2013, **52**, 171-180.
- 45 29. F. Kim, J. Y. Luo, R. Cruz-Silva, L. J. Cote, K. Sohn and J. X. Huang, *Advanced Functional Materials*,
46 2010, **20**, 2867-2873.
- 47 30. I. K. Moon, J. Lee, R. S. Ruoff and H. Lee, *Nature Communications*, 2010, **1**, 73.

- 1 31. Z. Sofer, P. Simek and M. Pumera, *Physical Chemistry Chemical Physics*, 2013, **15**, 9257-9264.
2 32. C. Z. Zhu, S. J. Guo, Y. X. Fang and S. J. Dong, *ACS Nano*, 2010, **4**, 2429-2437.
3 33. H.-L. Guo, X.-F. Wang, Q.-Y. Qian, F.-B. Wang and X.-H. Xia, *ACS Nano*, 2009, **3**, 2653-2659.
4 34. J. Chen, B. Yao, C. Li and G. Shi, *Carbon*, 2013, **64**, 225-229.
5 35. N. Liu, F. Luo, H. Wu, Y. Liu, C. Zhang and J. Chen, *Advanced Functional Materials*, 2008, **18**, 1518-
6 1525.
7 36. A. K. Geim, *Science*, 2009, **324**, 1530-1534.
8 37. Y. C. Si and E. T. Samulski, *Nano Letters*, 2008, **8**, 1679-1682.
9 38. S. Park, J. H. An, I. W. Jung, R. D. Piner, S. J. An, X. S. Li, A. Velamakanni and R. S. Ruoff, *Nano
10 Letters*, 2009, **9**, 1593-1597.
11 39. S. Park, J. H. An, R. D. Piner, I. Jung, D. X. Yang, A. Velamakanni, S. T. Nguyen and R. S. Ruoff,
12 *Chemistry of Materials*, 2008, **20**, 6592-6594.
13 40. M. Zhang, R. R. Parajuli, D. Mastrogiovanni, B. Dai, P. Lo, W. Cheung, R. Brukh, P. L. Chiu, T. Zhou,
14 Z. F. Liu, E. Garfunkel and H. X. He, *Small*, 2010, **6**, 1100-1107.
15 41. M. Lotya, Y. Hernandez, P. J. King, R. J. Smith, V. Nicolosi, L. S. Karlsson, F. M. Blighe, S. De, Z. Wang,
16 I. T. McGovern, G. S. Duesberg and J. N. Coleman, *J. Am. Chem. Soc.*, 2009, **131**, 3611-3620
17 42. K. H. Park, B. H. Kim, S. H. Song, J. Kwon, B. S. Kong, K. Kang and S. Jeon, *Nano Letters*, 2012, **12**,
18 2871-2876.
19 43. A. C. Jachak, M. Creighton, Y. Qiu, A. B. Kane and R. H. Hurt, *Mrs Bulletin*, 2012, **37**, 1307-1313.
20 44. V. C. Sanchez, A. Jachak, R. H. Hurt and A. B. Kane, *Chemical Research in Toxicology*, 2012, **25**, 15-
21 34.
22 45. V. Sridhar, J.-H. Jeon and I.-K. Oh, *Carbon*, 2010, **48**, 2953-2957.
23 46. P. L. Chiu, D. Mastrogiovanni, D. Wei, C. Louis, M. Jeong, G. Yu, P. Saad, C. R. Flach, R. Mendelsohn,
24 E. Garfunkel and H. X. He, *J. Am. Chem. Soc.*, 2012, **134**, 5850-5856.
25 47. M. A. Patel, H. Yang, P. L. Chiu, D. Mastrogiovanni, C. R. Flach, K. Savaram, L. Gomez, A. Hemnarine,
26 R. Mendelsohn, E. Garfunkel, H. Jiang and H. X. He, *Acs Nano*, 2013, **7**, 8147-8157.
27 48. K. J. Ziegler, Z. N. Gu, H. Q. Peng, E. L. Flor, R. H. Hauge and R. E. Smalley, *J. Am. Chem. Soc.*, 2005,
28 **127**, 1541.
29 49. J. Liu, A. G. Rinzler, H. J. Dai, J. H. Hafner, R. K. Bradley, P. J. Boul, A. Lu, T. Iverson, K. Shelimov, C.
30 B. Huffman, F. Rodriguez-Macias, Y. S. Shon, T. R. Lee, D. T. Colbert and R. E. Smalley, *Science*,
31 1998, **280**, 1253-1256.
32 50. A. M. Dimiev, S. M. Bachilo, R. Saito and J. M. Tour, *Acs Nano*, 2012, **6**, 7842-7849.
33 51. V. T. Tung, M. J. Allen, Y. Yang and R. B. Kaner, *Nature Nanotech.*, 2009, **4**, 25-29.
34 52. H. A. Becerril, J. Mao, Z. F. Liu, R. M. Stoltenberg, Z. Bao and Y. S. Chen, *ACS Nano*, 2008, **2**, 463-
35 470.
36 53. I. K. Moon, J. Lee, R. S. Ruoff and H. Lee, *Nat. Commun.*, 2010, **1**.
37 54. I. K. Moon, J. Lee, R. S. Ruoff and H. Lee, *Nat Commun*, 2010, **1**, 73.
38 55. Y. Hernandez, M. Lotya, D. Rickard, S. D. Bergin and J. N. Coleman, *Langmuir*, 2010, **26**, 3208-3213.
39 56. A. Bagri, C. Mattevi, M. Acik, Y. J. Chabal, M. Chhowalla and V. B. Shenoy, *Nature Chemistry*, 2010,
40 **2**, 581-587.
41 57. G. Eda, G. Fanchini and M. Chhowalla, *Nature Nanotech.*, 2008, **3**, 270-274.
42 58. D. Briggs and G. Beamson, *High Resolution XPS of Organic Polymers: The Scienta ESCA300
43 Database Appendix I.*, John Wiley & Sons Ltd., 1992.
44 59. G. E. Pike and C. H. Seager, *Phys. Rev. B*, 1974, **10**, 1421-1434.
45 60. H. Chen, M. B. Muller, K. J. Gilmore, G. G. Wallace and D. Li, *Advanced Materials*, 2008, **20**, 3557-
46 3561.
47 61. A. Bagri, R. Grantab, N. V. Medhekar and V. B. Shenoy, *Journal of Physical Chemistry C*, 2010, **114**,
48 12053-12061.

- 1 62. A. M. Dimiev and J. M. Tour, *Acs Nano*, 2014, **8**, 3060-3068.
2 63. T. H. Han, Y. K. Huang, A. T. L. Tan, V. P. Dravid and J. X. Huang, *Journal of the American Chemical*
3 *Society*, 2011, **133**, 15264-15267.
4 64. H. M. (Skip) Kingston and S. J. Haswell, eds., *Microwave-Enhanced Chemistry: Fundamentals,*
5 *Sample Preparation, and Applications*, American chemical society, Washington DC, 1997.
6 65. J. Zhang, H. L. Zou, Q. Qing, Y. L. Yang, Q. W. Li, Z. F. Liu, X. Y. Guo and Z. L. Du, *Journal of Physical*
7 *Chemistry B*, 2003, **107**, 3712-3718.
8 66. Wikipedia, 2014.
9 67. J. F. de Queiroz, J. W. D. Carneiro, A. A. Sabino, R. Sparrapan, M. N. Eberlin and P. M. Esteves,
10 *Journal of Organic Chemistry*, 2006, **71**, 6192-6203.
11 68. P. M. Esteves, J. W. D. Carneiro, S. P. Cardoso, A. G. H. Barbosa, K. K. Laali, G. Rasul, G. K. S. Prakash
12 and G. A. Olah, *Journal of the American Chemical Society*, 2003, **125**, 4836-4849.

13

14 **Figure Captions**

15 **Scheme 1.** Schematic drawing showing the process and oxidation mechanism of the proposed eco-
16 friendly approach to directly produce highly conductive, low oxygen containing graphene sheets.

17 A reversible H₂SO₄-GIC is formed by exposing graphite particles to a mixture of sulfuric acid and
18 (NH₄)₂S₂O₈. The enlarged distance between the individual graphene sheets and the positive
19 charges formed on their surfaces allow the purged molecular oxygen intercalating into the gallery
20 of the graphene sheets in the GIC. Upon microwave irradiation in a piranha solution, the atomic
21 oxygen generated from piranha and molecular oxygen intercalated inside the GIC synergistically
22 oxidize the graphene sheets both inside and outside of the GIC particles without releasing toxic
23 gases and generating aromatic small molecules as byproducts. This process rapidly generates
24 enough epoxy and other oxygen containing groups, which facilitate exfoliation of highly
25 conductive graphene sheets into water and other solvents without requirement of post-reduction
26 and surfactants for stabilization.

27 **Figure 1.** A representative STEM, SEM and AFM images of the Eco-ME-LOGr fabricated *via* 5
28 min O₂ purging of freshly prepared GIC, followed by 60 seconds microwave irradiation in piranha

1 solution (A-C). Panel D shows an AFM picture of Eco-ME-LOGr sheets fabricated *via* microwave
2 irradiation of graphite particles in piranha solution.

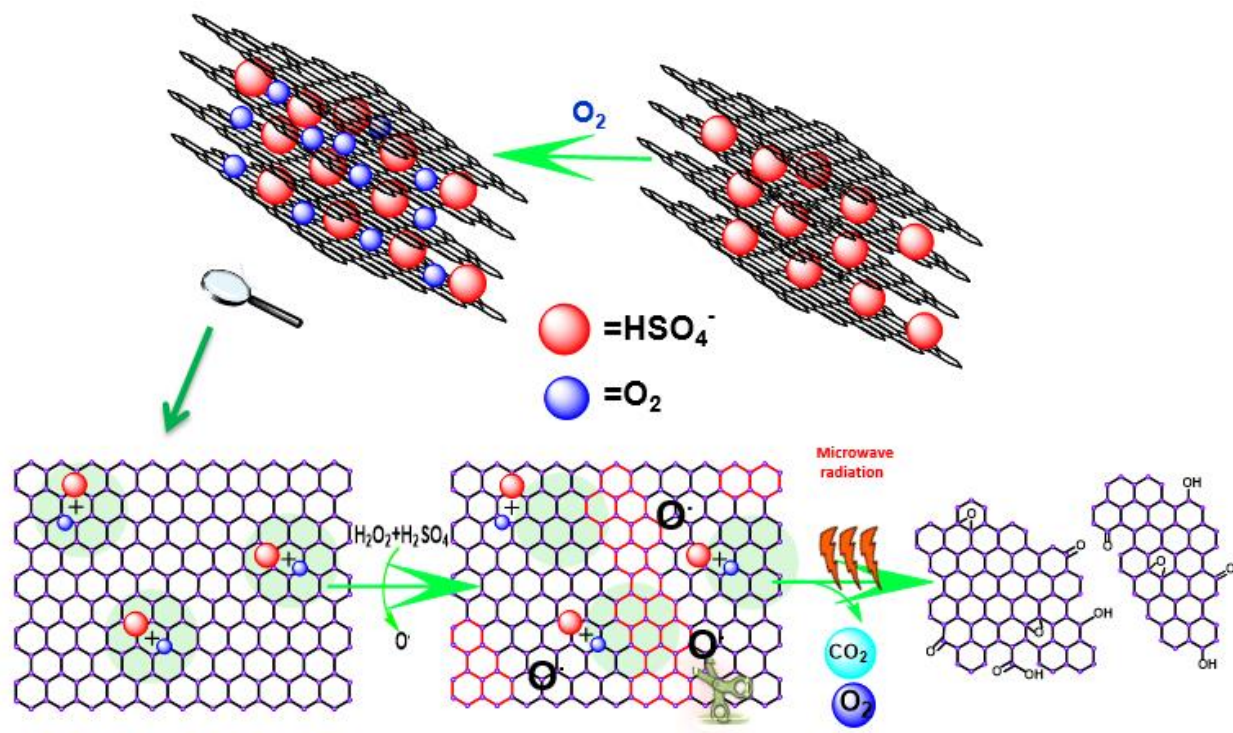
3 **Figure 2.** (A) Uv-Vis-Near Infrared spectroscopy of the Eco-ME-LOGr and graphene oxide
4 dispersion in water and their digital pictures (Inset). (B) Raman spectroscopy of the Eco-ME-LOGr
5 films on alumina anodic membrane.

6 **Figure 3.** Digital pictures of graphene dispersion in different solvents. The dispersions on the top
7 are fabricated *via* the Eco-friendly approach and the bottom ones were fabricated *via* nitronium
8 oxidation.

9 **Figure 4.** XPS spectra of Eco-ME-LOGr films and ME-LOGr films on Au substrates. Panel A and
10 B is C1s and O2p signal from the Eco-ME-LOGr films. The O2p signal from ME-LOGr film was
11 displayed here for comparison.

12 **Figure 5.** Electronic percolation of the Eco-ME-LOGr films prepared by vacuum filtration.

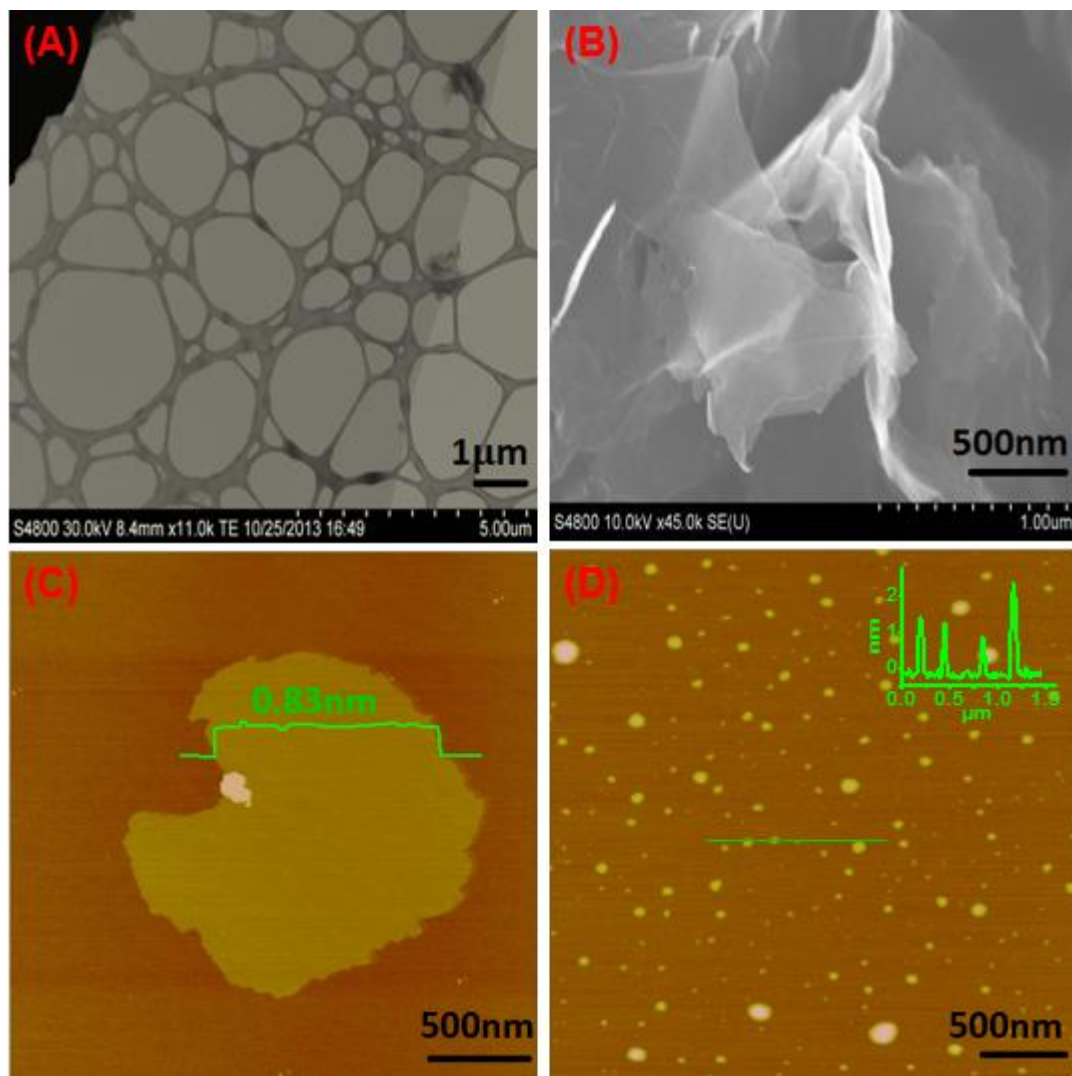
13 **Figure 6.** (A) MS spectrum of the exhausted gas collected during microwave irradiation *via* the
14 Eco-friendly approach. (B) GC spectra of the filtrates collected during cleaning of the microwaved
15 products. The curves from top to bottom are for the filtrates from nitronium oxidation, the Eco-
16 friendly approach, and a control experiment *via* the eco-friendly approach without adding graphite
17 particles during microwave irradiation, and pure THF solvent. Inset: Digital Pictures of the two
18 filtrates.



1

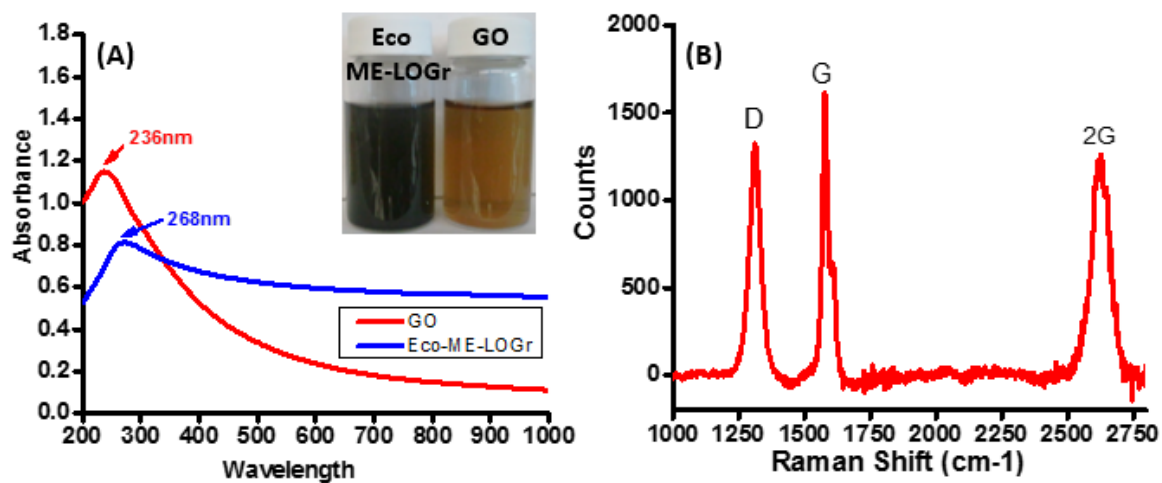
2 **Scheme 1.**

3

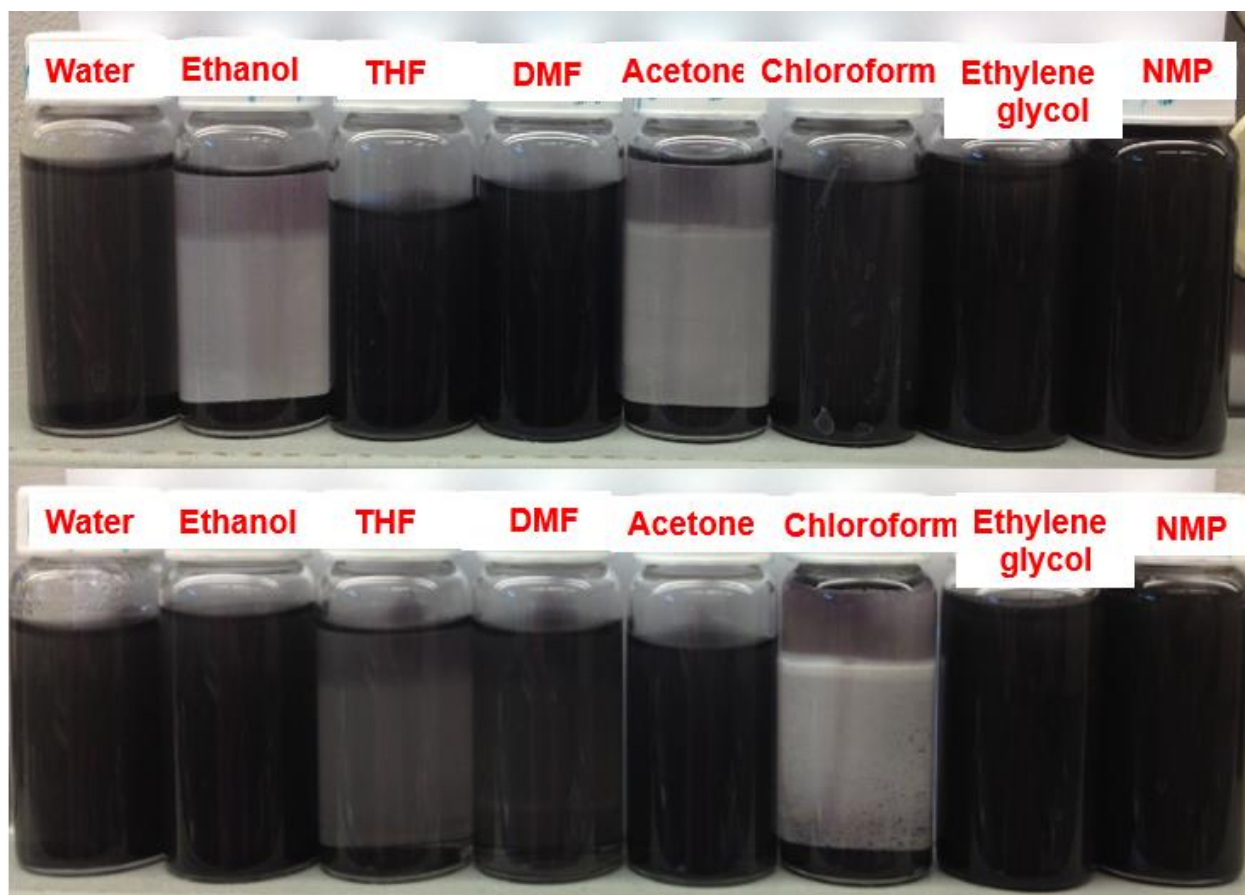


1

2 **Figure 1.**

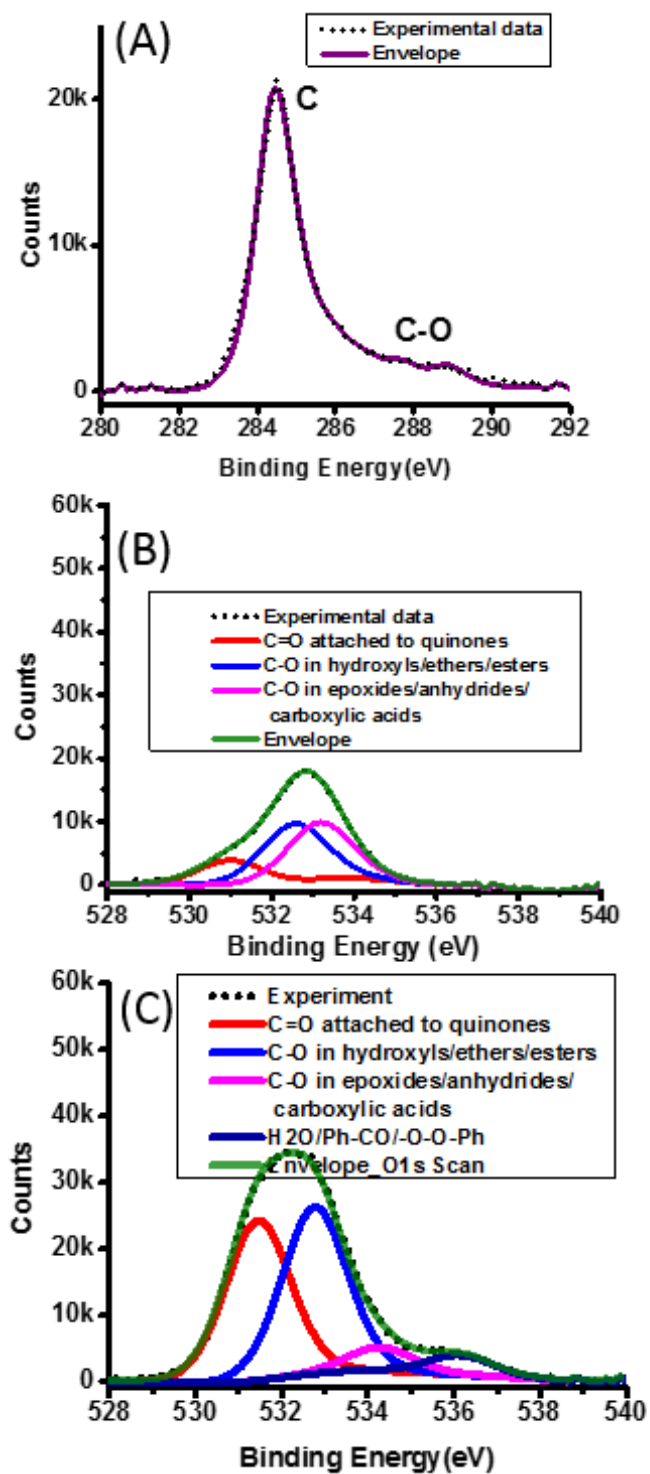


1

2 **Figure 2.**

3

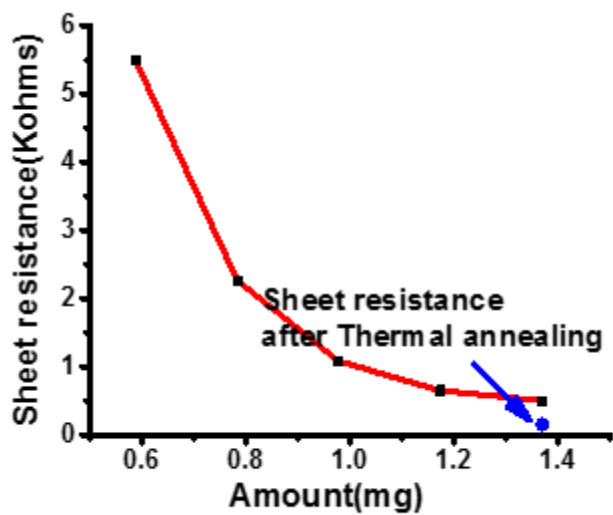
4 **Figure 3.**



1

2 Figure 4.

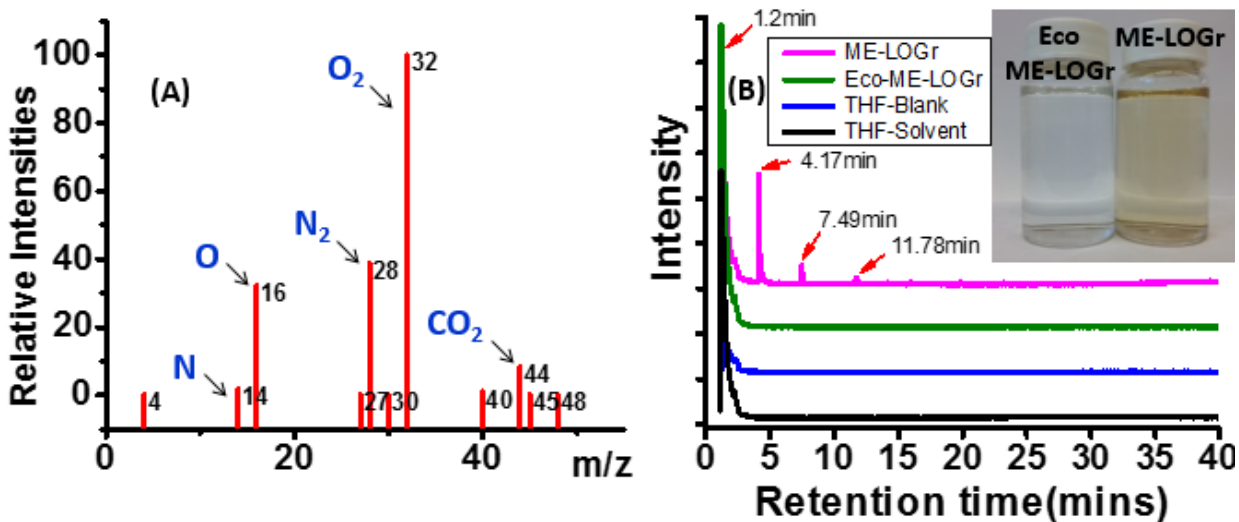
3



1

2 Figure 5.

3



4

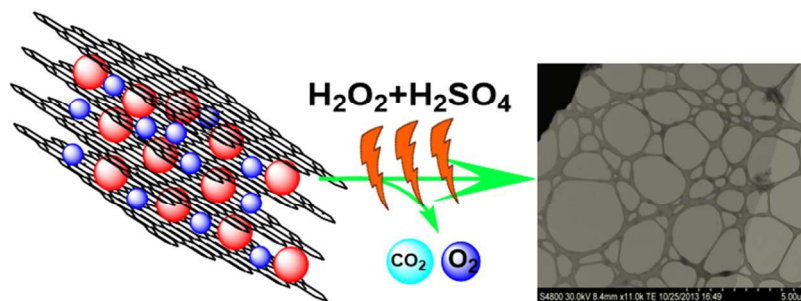
5 Figure 6.

6

7

8

Table of Contents



Ecofriendly approach for Graphene fabrication, no toxic and metal containing compounds were used, and no toxic byproducts were generated.

Supplementary materials

Synergy of Oxygen and Piranha Solution for Eco-Friendly Production of Highly Conductive and “Clean” Graphene Dispersions

Keerthi Savaram,¹ Malathi Kalyanikar,² Mehulkumar Patel,¹ Roman Brukh,¹ Carol R. Flach,¹ Ruiming Huang,¹ M.Reza Khoshi,¹ Richard Mendelsohn,¹ Andrew Wang,³ Eric Garfunkel,² and Huixin He^{1*}

¹Chemistry Department, Rutgers University, Newark, NJ 07102; ²Department of Chemistry and Chemical Biology, Rutgers University, 610 Taylor Rd, Piscataway, NJ 08854; Ocean Nanotech LLC, 7964 Arjons Drive, Suite G, San Diego, CA 92126.

The Greenness of the present Graphene Fabrication technique can be attributed to the following pointers:

1. Metal oxidizing agents such as KMnO_4 ,¹ KClO_3 ,² NaNO_3 ,¹ etc are not used in this synthesis technique and hence the additional solvents (HCl , H_2O_2) needed to wash away the unreacted metals can be excluded.
2. Since the as-fabricated graphene sheets are highly conductive, post treatment is not necessary where either a reductions process or thermal annealing is required to render the GO conductive.
3. The energy needed for the reaction to proceed is 1.8×10^4 Joules of energy (5kWh) using the CEM discover microwave (300W of power is used for 60sec) which is very low when compared to the traditional heating in an oil bath which requires approximately around 3.79×10^5 Joules of energy (103KWh) (where 630W of power is used for 10mins to reach 100°C and then the power is used accordingly to maintain the temperature for as long as

2hrs to 5days). This makes the microwave approach an energy saving and economical approach.

4. In this ecofriendly approach mentioned, toxic gases such as CO, NO₂, N₂O₄ are not produced and the filtrate does not contain any small molecules which pose as a hazard to the environment.³
5. In this ecofriendly approach mentioned, the time required for graphene fabrication is very short *i.e* 60sec when compared to the traditional GO synthesis 2hrs to 5days and in addition they need to be further reduced to be converted to rGO.⁴

Supplemental Experimental results

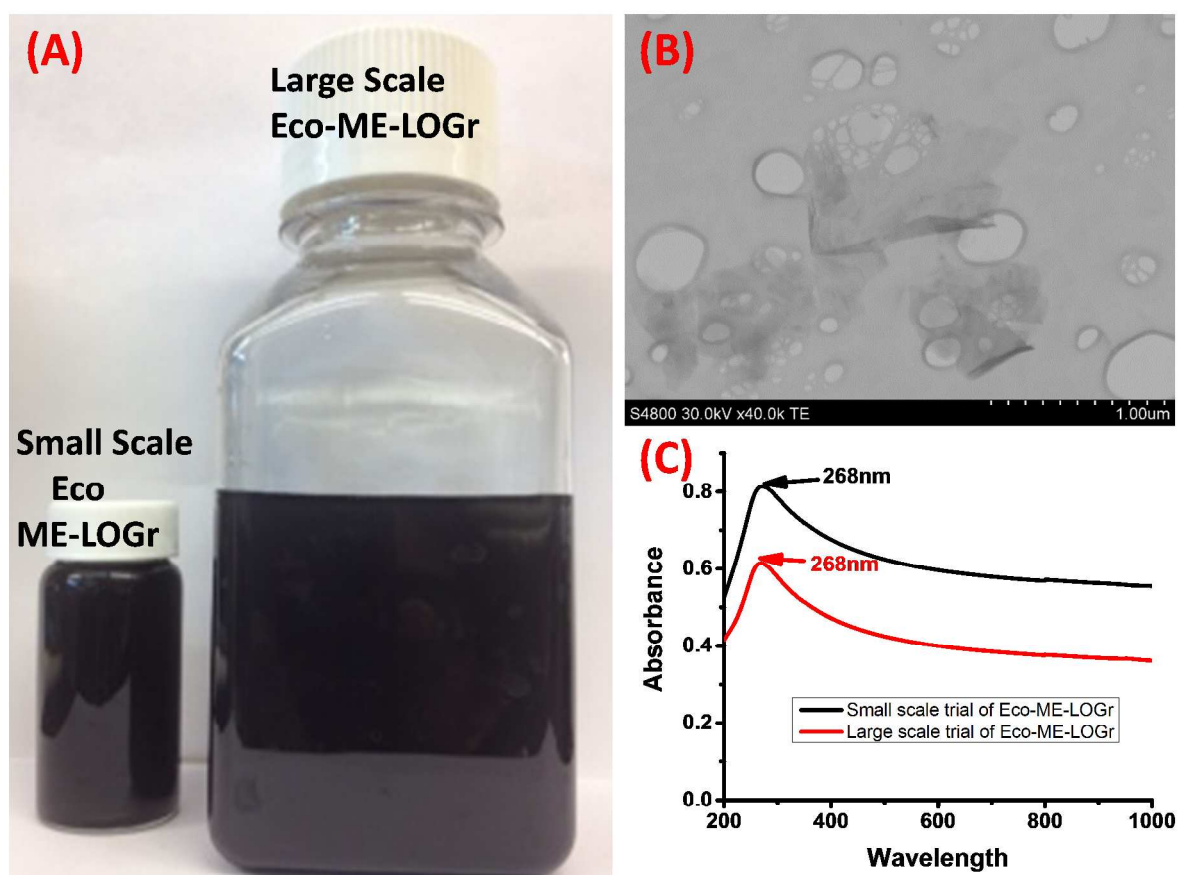


Figure S1: (A). Digital photographs of the stable Eco-ME-LOGr dispersions in water from small and larger scale production. (CEM discover, 300 watts for small scale, and Synthwave from Milestone, 900W for larger scale production, see details in the experimental section) in a piranha

solution. (B) A representative STEM image of the graphene sheets from larger scale production achieved via Synthwave from Milestone. (C) UV-Vis-NIR spectra of the Eco-ME-LOGr in water from small and larger scale production. The similar lateral sizes of the graphene sheets, and the overlapping of the two UV-Vis-NIR spectra indicate that similar quality of graphene sheets were obtained, demonstrating that this Eco-Friendly approach can be easily scaled up for mass production.

Table S1 Concentration and production yield of the Eco-ME-LOGr in various solvents

Solvent	Concentration (mg/ml)	Total weight in the solution	Initial weight(mg)	% yield
Ethylene glycol	0.40	16.12	20	80.6
NMP	0.29	11.43	20	57.2
Water	0.22	10.27	20	51.4
DMF	0.20	8.02	20	40.1
Chloroform	0.19	7.56	20	37.8
THF	0.071	2.84	20	14.2
Acetone	0.026	1.05	20	5.3

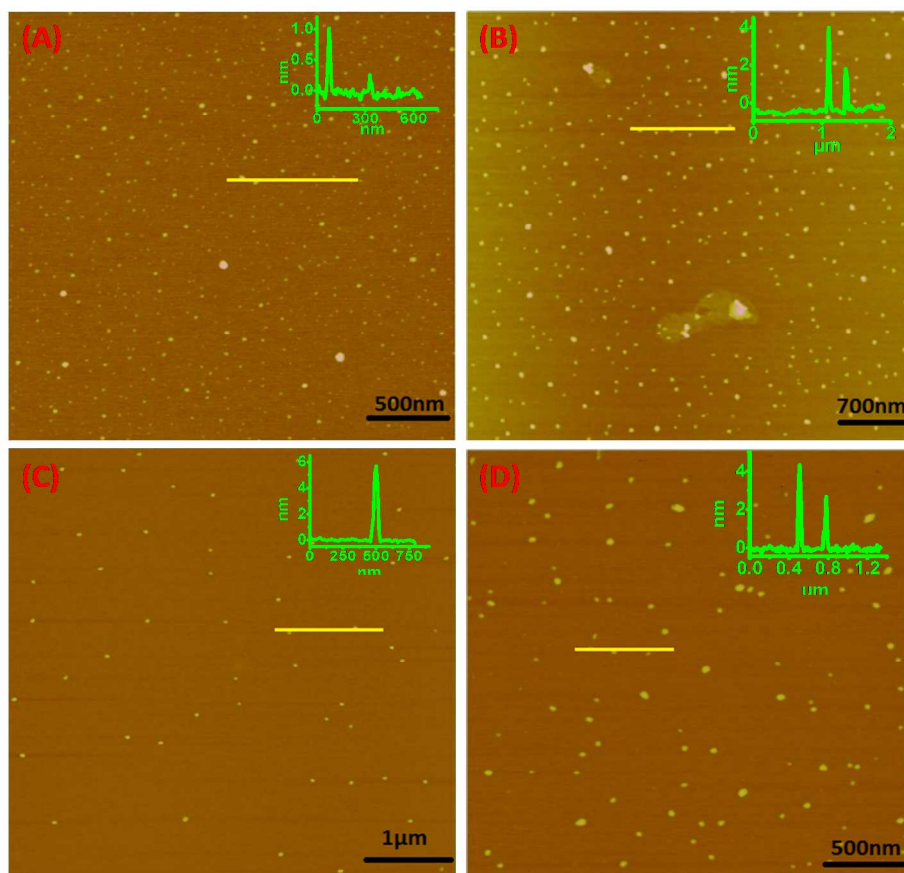


Figure S2. AFM images of graphene sheets prepared from fresh GIC without O₂ purging (A); GIC purged with 20 minutes O₂ (B); GIC with 5 minutes O₂ purging, but longer microwave irradiation (75 second, instead of 60 seconds) (C); GIC with 5 minutes O₂ purging with traditional heating instead of microwave heating (D).

Table S2. Weights of Graphite and GICs with/ and without purging with 5 min of O₂ after washing with water.

Reaction mixtures	Initial weight(mg)	Weight after washing(mg)
Fresh GIC	40.1mg	40.2mg
Fresh GIC purged with O ₂	40mg	41.6mg

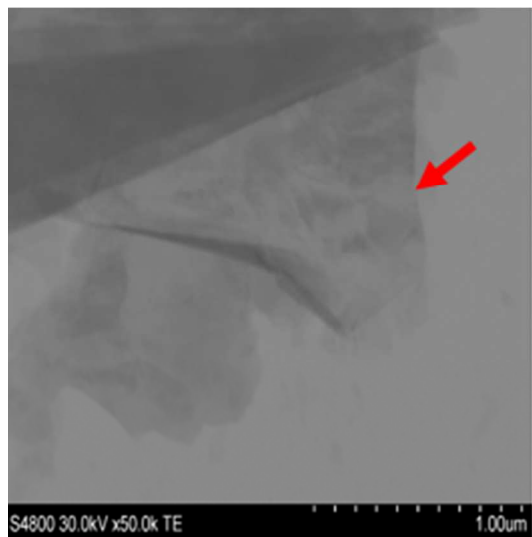


Figure S3. A typical STEM images of graphene structures obtained by microwave irradiation of oxygen purged GIC without further addition of piranha solution. The image shows thick graphene sheets with straight edges indicated by the arrow.

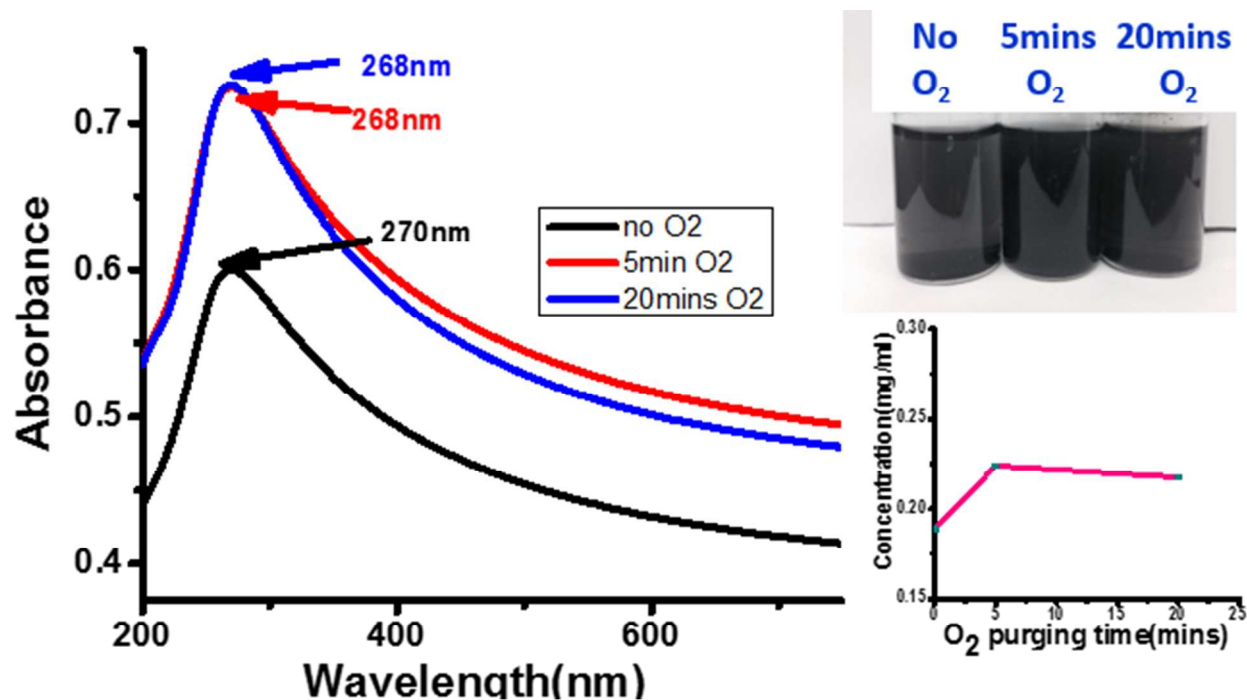


Figure S4. UV-Vis spectra and digital pictures of the dispersed graphene solution to show the yield of the products depends on the O₂ purging time with the same microwave power (300 W).

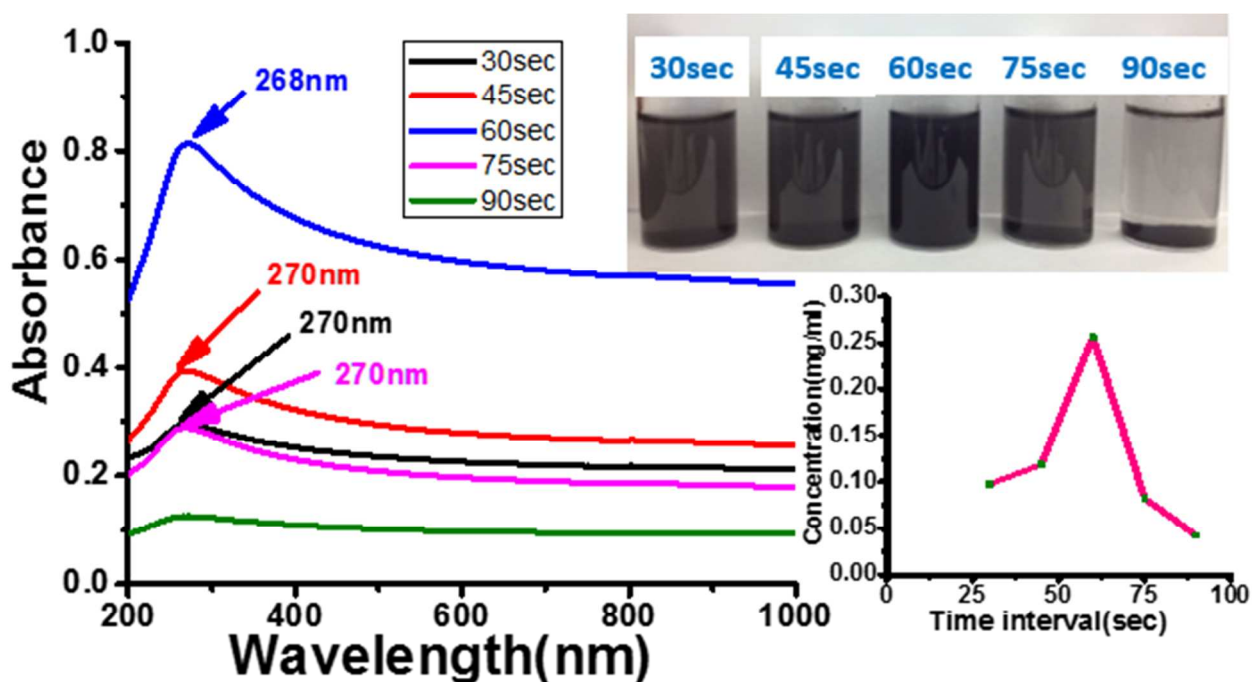


Figure S5. UV-Vis spectra and digital pictures of the dispersed graphene solution to show the yield of the products depends on the microwave irradiation time with the same microwave power (300 W). With 60 second of irradiation, the concentration of the dispersed graphene sheets reached the maximum.

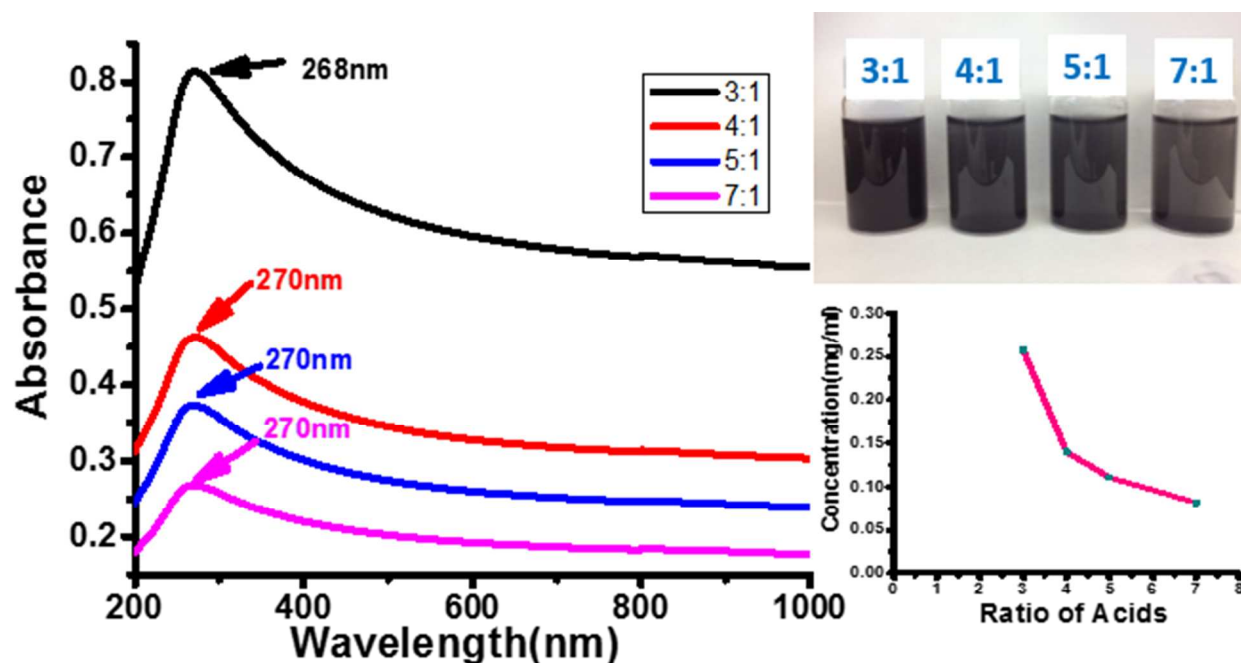


Figure S6. UV-Vis spectra and digital pictures of the dispersed graphene solution to show the yield of the products depends on the ratio of H₂SO₄ to H₂O₂ of the piranha solutions, with 3:1 ratio giving the highest production yield (Microwave irradiation time 60 seconds and microwave power of 300 W).

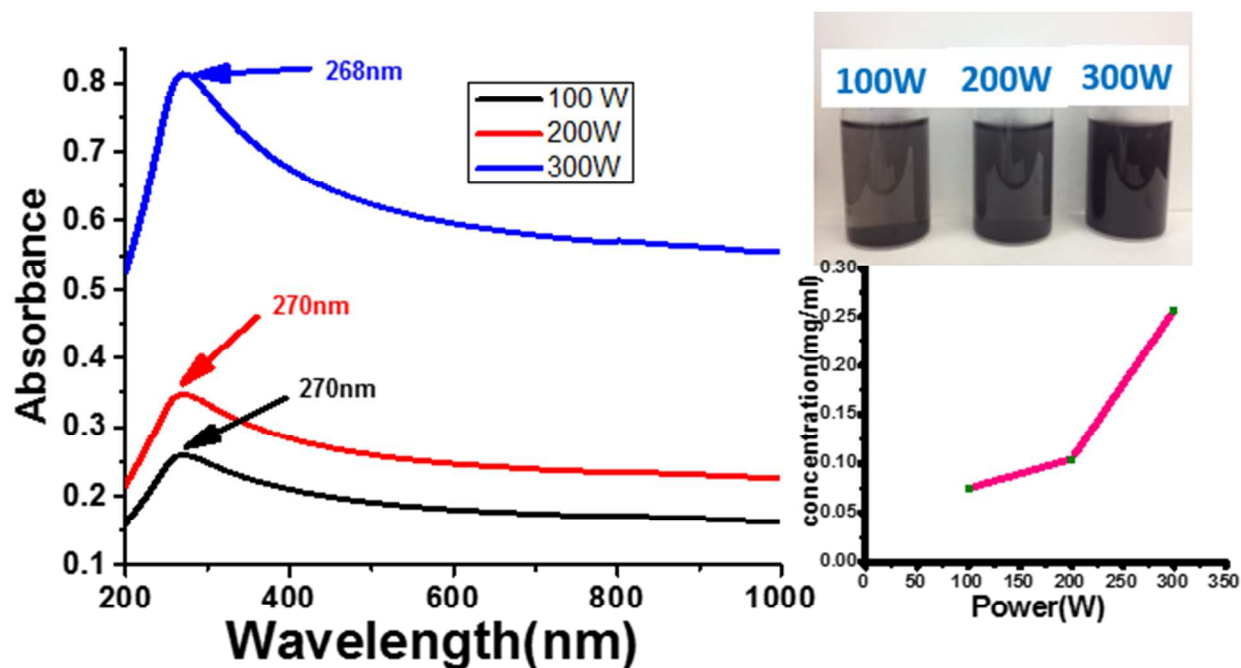
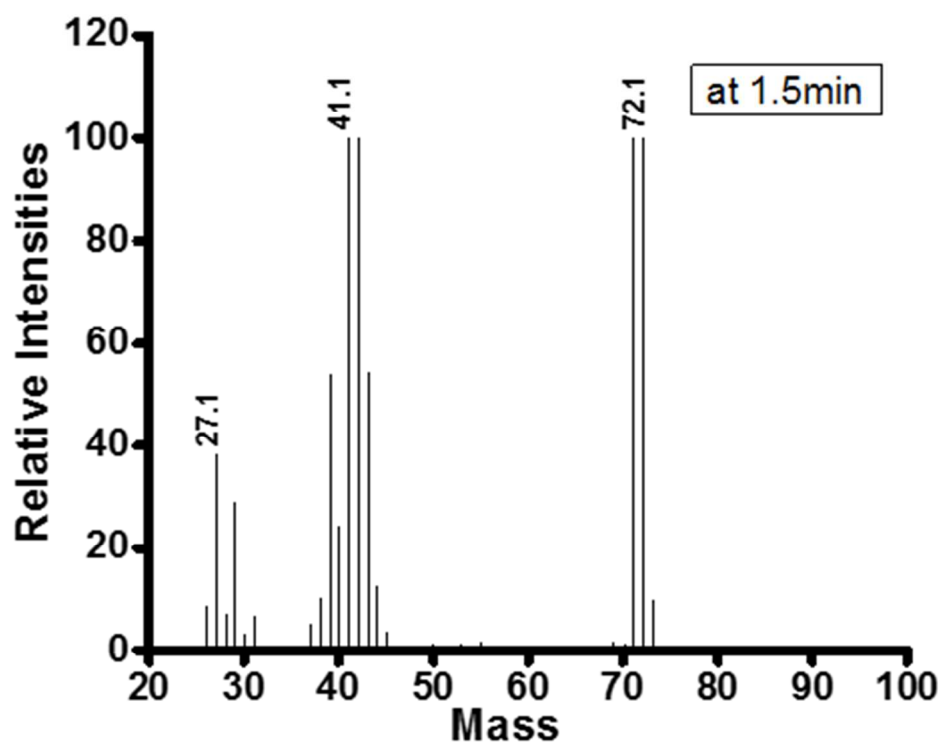
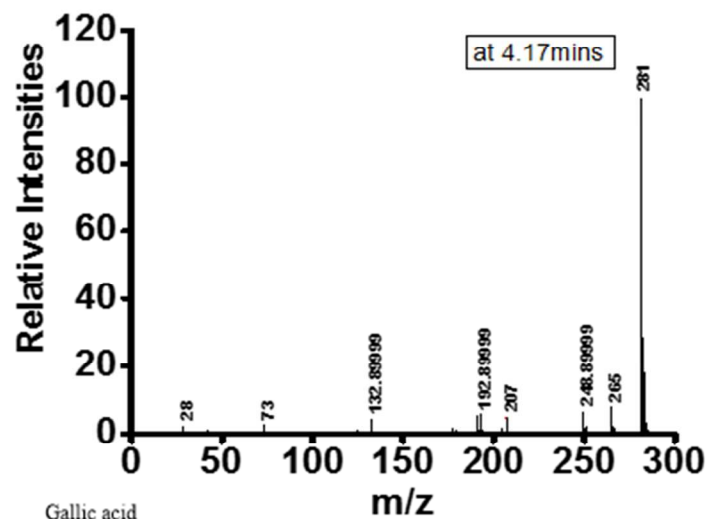


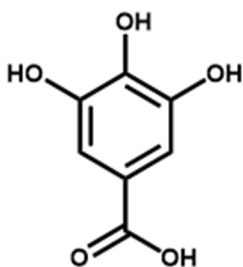
Figure S7. UV-Vis spectra and digital pictures of the dispersed graphene solution to show the yield of the products depends on the microwave power.

Figure S8. Mass Spectra at different retention time in the GC spectrum showing in Figure 6B.

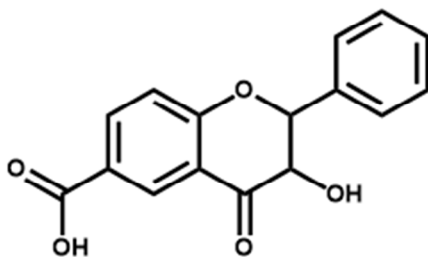




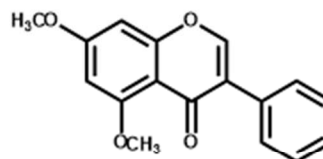
Gallic acid
MW 170.02
C₇H₆O₅
score 0.64
hit 36



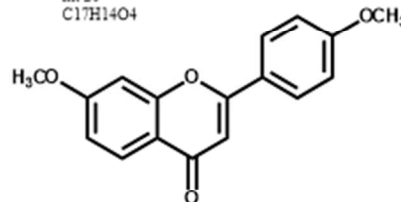
6- carboxy flavanol
Mw 282.053
C₁₆H₁₀O₅
score 0.76
hit 23



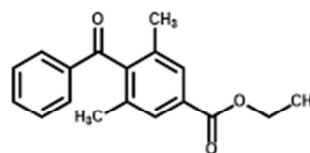
5,7 dimethoxy isoflavone
score 0.71
hit 24
C₁₇H₁₄O₄



4,7 dimethoxy isoflavone
score 0.66
hit 20
C₁₇H₁₄O₄



Ethyl 4 benzoyl 3,5 dimethyl benzoate
Mw 282.126
C₁₈H₁₈O₃
Score 0.79
hit 46



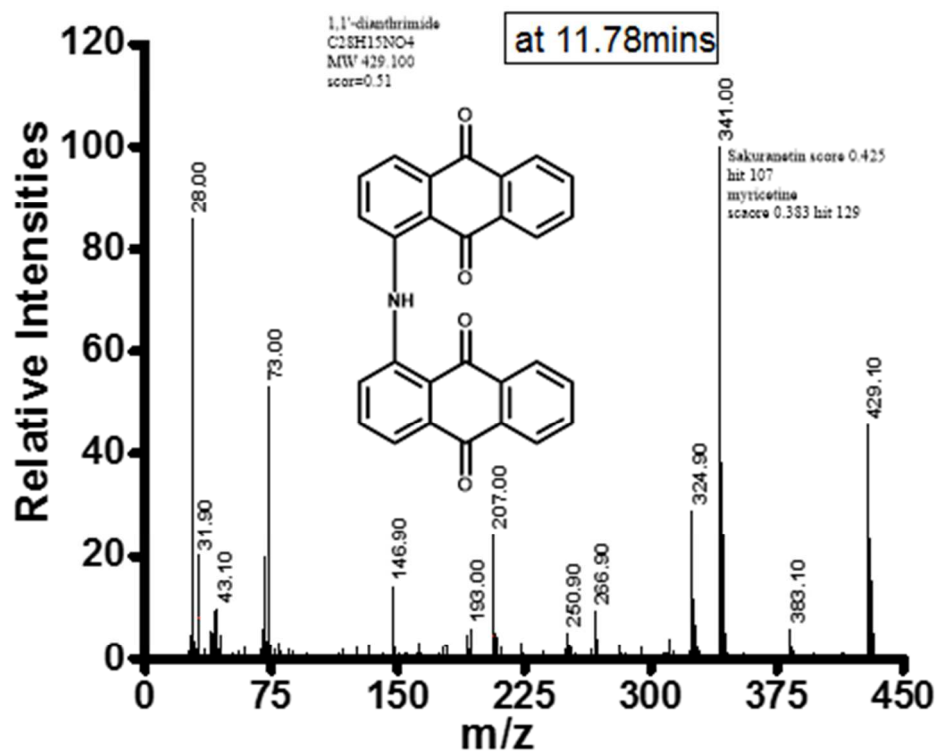
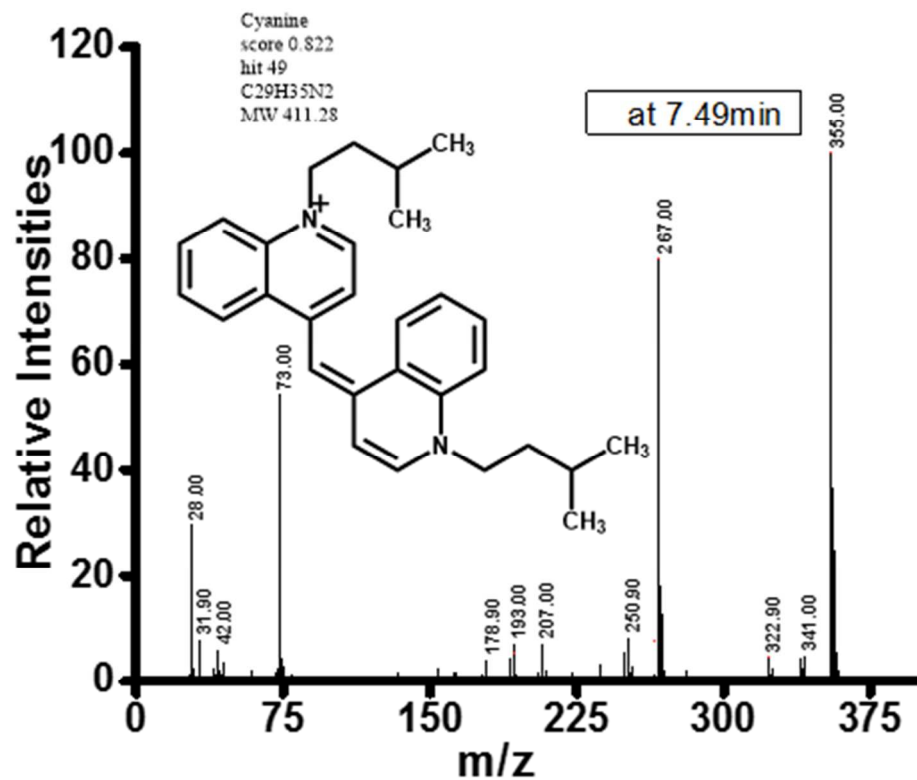


Table S3 Detailed molecular structures and their score compared to the mass spectra in the mass bank database.

Name	Molecular weight	Mass Bank Score	Structure
Ethyl 4 benzoyl 3,5 dimethyl benzoate	282.126	0.79	
6-Carboxy Flavanol	282.053	0.77	
5,7 dimethylisoflavone	282.089	0.71	
4',7 dimethoxy isoflavone	282.089	0.66	
Gallic acid	170.02	0.65	
Cyanine	411.280	0.82	
Gentisic acid	156.027	0.82	
3,4 di hydroxy mandelic acid	184.15	0.81	
2,3 dihydroxy benzoic acid	154.12	0.80	

Sample Preparation for characterization:**Surface Morphology:**

Atomic Force Microscopy (AFM): AFM helps to determine the size and thickness (height) of the graphene sheets synthesized. The AFM samples were prepared by dropping 1-2 μ l of the dispersed graphene solution onto freshly cleaved mica surface and then allowing it to dry. The sample after drying is washed with water drop by drop to remove the dirt on the sample if by any chance accumulated and again dried. This sample is scanned using a Nanoscope IIIa multimode SPM (Digital instruments) with a J scanner for small scan size and G scanner for larger scan size operated in "Tapping mode". The AFM tips for imaging were 160 μ m long rectangular silicon cantilever/tip assembly from AppNano was used with a resonance frequency of 160 kHz and a spring constant of approximately 7.7N/m with a tip radius of less than 10nm.

Scanning Electron Microscopy (SEM) and scanning Transmission Electron Microscopy (STEM): SEM samples were prepared by dropping 1-2 μ l of the sample onto silica substrate. The silica substrate is cleaned initially with piranha solution and then water and then dried with N₂ gas. The sample solution is dropped onto silica substrate and then allowed to dry for 2-3mins and then dried in N₂ gas to spread the sample throughout the substrate. The SEM images were captured using a Hitachi S-4800 Field Emission Scanning Electron Microscope (FE-SEM, Hitachi Co.Ltd.) under an accelerating voltage of 1-2KV and a probe current of 10 μ A to obtain images with high contrast. STEM samples were prepared by dropping 1 μ l of the sample on the Cu grid. After the samples are dried in air, they are imaged with a Hitachi S-4800 FE SEM under high accelerating voltage of 30KV and a probe current of 10-15 μ A with a working distance of 15mm.

X ray photoelectron Spectroscopy (XPS): XPS was pursued by depositing graphene solution onto a gold film of $1 \times 1 \text{ cm}^2$ surface area. The deposited film has a thickness roughly 50nm. XPS data was acquired using a thermo scientific $K\alpha$ system with a monochromated Al $K\alpha$ X-ray source ($h\nu=1486.7\text{ev}$).

Raman Spectroscopy: Raman spectra is a more direct and non-destructive method which gives useful information about the quality of the graphene sheets. Raman spectra from films deposited on Alumina membranes were collected with a Kaiser Optical Systems Raman Microprobe with a 785nm solid state diode laser, the collection time is 60sec for each spectrum and collected three times on an average.

Optical and Electronic properties:

Cary UV-VIS spectroscopy 5000: The optical properties of the graphene dispersions were measured by the UV-VIS NIR spectroscopy. The spectra were obtained from Cary-5000 Ultra violet-Visible-Near Infrared Spectroscopy operated in double beam with 200-1000nm wavelength range.

Conductivity measurements:

First the sheet resistance of graphene films with controlled thicknesses was prepared by a vacuum filtration method through alumina anodic membranes (Whatman Ltd) with $0.2 \mu\text{m}$ pores. These films were dried in vacuum for 1 day to remove the residual solvent before conductivity measurements. The sheet resistance is measured by a manual four point resistivity probe from Lucas Laboratories, model 302. The conductivity of the films is calculated from the sheet resistance and thickness by the formula:

$$\text{Conductivity} = \frac{1}{\text{Sheet resistance} \times \text{thickness}}$$

This formula can be used to measure the films with thickness not more than half of the probe spacing (the distance between two probes of the four point probe instrument). The error in this case is less than 1%.

Rutherford Back Scattering technique for thickness measurement: The thickness of the film to obtain the conductivity in S/m for a given film of known sheet resistance is determined by Rutherford backscattering technique (RBS). Rutherford back scattering (RBS) was performed using a 2 MeV He²⁺ ion beam produced in a tandem accelerator with an ion current of 2–3 nA. Spectra were collected in the back scattering geometry and simulations were performed using the SIMNRA program (see detail in supplementary materials). The samples were prepared via vacuum filtration on Anodisc membranes and then transferred onto Si surface after etching the membrane in a strong base NaOH (4M), followed by washing with excess water until the pH of the solution becomes neutral. After transferring to Si surface, the samples were dried in vacuum and then the thickness of them is measured using RBS.

Gas Chromatography-Mass Spectrometry (GC-MS). The gas evolved during the reaction process is carefully collected through a syringe and 1ml of the gas sample taken from the headspace (total headspace volume: 5 mL) was injected into an Agilent HP6890 system, which was equipped with a HP-5-MS capillary column. For the filtrate, 10 μ l of the THF extracts was injected into the same GC-MS system by sampling through the septum of one of the four vials (THF extracts of the filtrate from nitronium oxidation approach, the filtrate from this Eco-friendly approach, and the filtrate from a control experiment *via* the Eco-friendly approach without adding graphite particles, and pure THF solvent. A temperature program was performed,

starting at 50 °C held for 1 min, followed by temperature ramping at a rate of 10 °/min to a final temperature of 300 °C and held for an additional 1 min.

Rutherford Back Scattering (RBS)

For a given film of known sheet resistance, the conductivity can be analyzed as a function of its thickness. The thickness measurement of such thin films is characterized by the Rutherford backscattering spectroscopy (RBS) technique. Eco-ME-LOGr samples with varying thickness on silicon-oxide/silicon were analyzed. The measurements provided the elemental composition and the thickness of the various films under study.

Principle: For RBS measurement, we used a well collimated monoenergetic beam of He²⁺ ions directed onto and scattered from the target atoms (in the sample) due to coulombic repulsion between the nuclei. The kinematics of the collision determine the energy of the scattered He²⁺ ion, which is less than its energy prior to collision (with the excess energy going into the recoiled atom/ion). We used an incident energy of approximately 2MeV. The He²⁺ ion energy loss during scattering depends on the mass of the target nucleus and the scattering angle. Additional energy is lost while passing through the film which gives rise to the depth sensitivity. Thus by monitoring the number of backscattered ions as a function of energy, the elemental composition and the depth distribution of elements can be determined. SIMNRA software is used to simulate the experimental spectra. If there is a good correlation between experimental and simulated data, then the simulation can be used to offer an accurate determination of the film thickness.

Eco-ME-LOGr samples with varying thicknesses on silicon-oxide/silicon were analyzed. The thickness of these films varied from 90 to 20nm depending on the quantity of the deposited material. With decreasing thickness the sheet resistance increased, as anticipated.

Data treatment

To illustrate the data treatment, a sample spectrum (Eco-ME-LOGr film on the substrate) is considered as shown in Figure S9. The spectrum shows the backscattered He²⁺ ions displayed in terms of energy channels. For the thickness calculation, the following procedure is utilized.

The *target* parameter in SIMNRA⁵ software is the main parameter in controlling the simulated spectrum. For the sample, a total of 3 layers is considered with its elemental composition as follows: (1) Layer 1 consists of Eco-ME-LOGr hence the elemental composition are made of C and O (2) Layer 2 consists of Si and O (3) Layer 3 consists of Si (large thickness) from the substrate. The thickness and concentration parameters under *target* are varied to simulate the experimental data. Once a good fit is obtained under the *density calculation* parameter in SIMNRA, specifying the abundant element in the topmost layer (Layer1) displays the atomic

density and this value is used for the thickness calculation. Thus, the product of the atomic density and the displayed layer thickness in terms of areal density provides a good approximation of the film thickness. There is some uncertainty in our total quantification due to small amount of oxygen present, which is not considered in the density but this is small and included as error in the thickness determination.

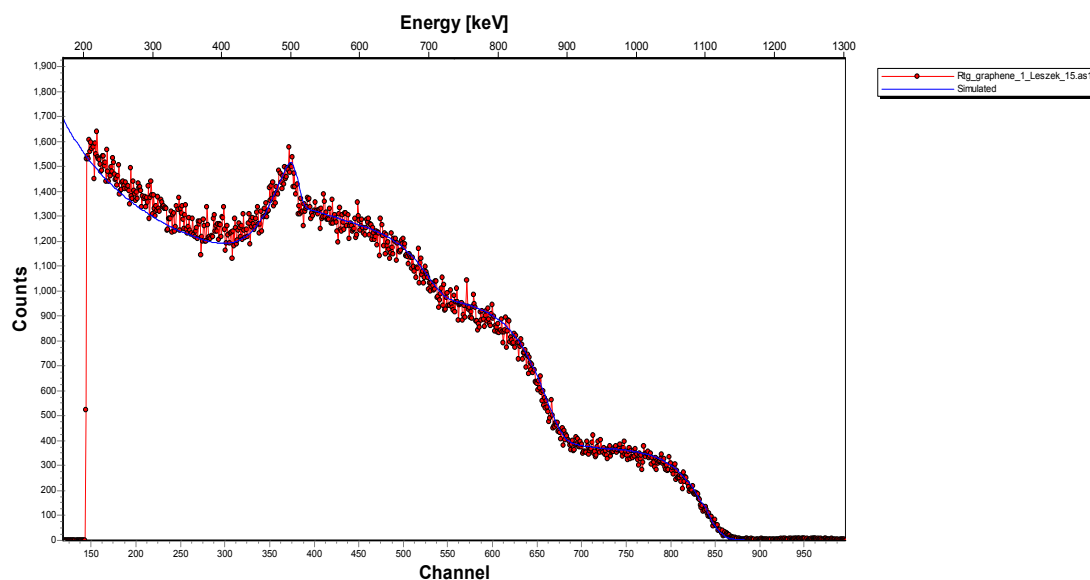


Figure S9 – SIMNRA simulated curve (blue) fitted to experimental data (red) with different elements in the sample

In another Ion beam based method to obtain the thickness, the difference in the leading edge between the pure substrate and the substrate with Eco-ME-LOGr film is analyzed as shown in Figure S10. The energy shift between the leading edges along with the stopping factor (from SRIM) gives the film thickness.

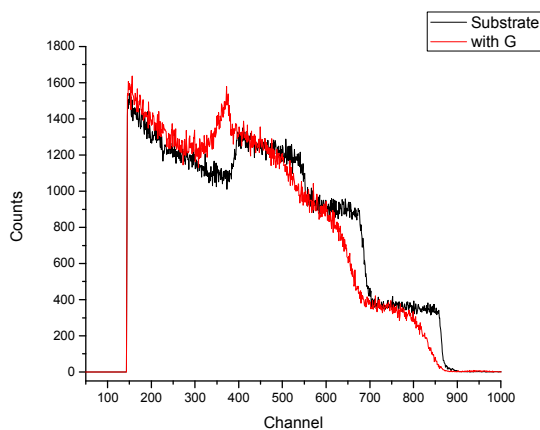


Figure S10 – Pure substrate (black) and substrate and film (Red) overlay of RBS spectra

Both these methods display a similar trend in the analysis of the various samples and the trend for the different thicknesses are shown in Table S4. The error for samples with thinner films is a little higher (8%) relative to the samples with thicker films (5%).

Thickness calculation of Eco-ME-LOGr film		
Sample	From SIMNRA (nm)	Using leading edge (nm)
1	88 ± 4	84 ± 3
2	75 ± 4	66 ± 3
3	66 ± 3	46 ± 2
4	44 ± 2	31 ± 1
5	42 ± 2	33 ± 1
6	26 ± 2	18 ± 1

Table S4. Thickness calculation of Gr film using two different methods.

X-ray Photoelectron Spectroscopy (XPS)

XPS characterization was performed after depositing Eco-ME-LOGr solution onto a gold film (The solution was drop casted onto the gold substrate repeatedly until sufficient thickness is achieved). XPS spectra were acquired using a Thermo Scientific K-Alpha system with a monochromated Al K α x-ray source ($h\nu = 1486.7$ eV) and a hemispherical analyzer. The energy calibration was performed in-situ with respect to the Au substrate with the sample. The reference value of Au 4f 7/2 peak centered at a binding energy of 84.2 eV with a FWHM of 1.0 eV was used for calibrating the Au substrate. Energy shifts for normalizing with respect to the calibrated Au peak were not required as no charging was observed.

Casa XPS was used for the peak-fitting. For all the spectra, a Shirley background removal was applied followed by a Gaussian-Lorentzian hybrid function to fit individual peaks. The FWHM of deconvoluted peaks are a combination of intrinsic photoelectron core-hole lifetimes, instrumental broadening and film heterogeneity. Therefore; the FWHM was allowed to float within a narrow range to accommodate these effects. For carbon peaks, 0.9-1.2 eV was utilized whereas 1.6-1.9 eV was used for oxygen. Relative binding energies for the different carbon species were obtained from the work of Briggs and Beamson, and are related to the absolute energy value for adventitious carbon, as noted above⁶. The graphitic carbon peak was assigned a fixed energy of 284.2 as per the literature value of HOPG.⁷ Further analysis was performed to analyze the specific bonding present in each material. The oxygen free carbon is mainly derived from the C 1s peak of aromatic rings (284.2 eV), and that of the aliphatic rings and/or linear alkylinic carbon chains (284.7 eV). The peaks for oxygen containing carbon with various

functionalization are assigned as follows: C-OC and C-OH (285.8 eV), C-OC=O (287.5 eV), C=O and O-C-O (288.7 eV), O-C(=O)-O (289.7 eV)³.

References

1. W. S. Hummers and R. E. Offeman, *J. Am. Chem. Soc.*, 1958, **80**, 1339-1339.
2. L. Staudenmaier, *Berichte Der Deutschen Chemischen Gesellschaft*, 1898, **31**, 1481-1487.
3. P. L. Chiu, D. Mastrogiovanni, D. Wei, C. Louis, M. Jeong, G. Yu, P. Saad, C. R. Flach, R. Mendelsohn, E. Garfunkel and H. X. He, *J. Am. Chem. Soc.*, 2012, **134**, 5850-5856.
4. O. C. Compton and S. T. Nguyen, *Small*, 2010, **6**, 711-723.
5. <http://home.rzg.mpg.de/~mam/>.
6. D. Briggs and G. Beamson, *High Resolution XPS of Organic Polymers: The Scienta ESCA300 Database Appendix I.*, John Wiley & Sons Ltd., 1992.
7. J. F. Morar, F. J. Himpsel, G. Hollinger, J. L. Jordan, G. Hughes and F. R. McFeely, *Physical Review B*, 1986, **33**, 1340-1345.